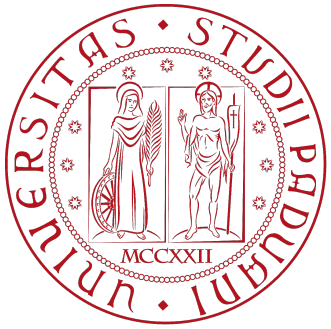

Università degli Studi di Padova

Dipartimento di Ingegneria Industriale DII

Corso di Laurea Magistrale in Ingegneria Aerospaziale

Determination of on-board accelerometer's characteristics for the METRIC mission

Relatore:
Prof. Lorenzini Enrico
Correlatore:
Prof. Valmorbida Andrea

Laureando:
Anese Giovanni
2004158

Anno Accademico 2021/2022

Abstract

METRIC is a proposed mission that aims to improve the knowledge of atmospheric density, general relativity and geodesy. The mission foresees a small spherical satellite placed in a polar eccentric orbit, with the apogee at 1200 km of altitude and perigee at 450 km. The spacecraft will be tracked from ground and space and have an on-board accelerometer. The last one will measure non-gravitational accelerations (namely due to drag and solar radiation pressure). A dynamical simulator has been implemented with known models (e.g. gravitational model, NRLMSISE-00), so that, through some simulations, it's possible to estimate the non-gravitational accelerations acting on the satellite. These are then analyzed in order to extract their principal characteristics: intensity and frequency spectrum. In this way accelerometer's features - dynamic range, required accuracy and frequency bandwidth- can be determined in order to have useful measurements. The data collected by the accelerometer will be used, also with POD data that comes from tracking, to improve the models of atmospheric density and general relativity.

Contents

1 Introduction **1**

2 Missions for near-Earth environment **3**
2.1 LAGEOS and LARES 3
2.2 CHAMP 4
2.3 GRACE 4
2.4 GOCE 5

3 METRIC mission **7**
3.1 METRIC goals 7
3.2 METRIC orbit 8
3.3 Satellite and on-board instruments 9

4 Dynamical model **11**
4.1 Software: Matlab© & GMAT 11
4.2 Mathematical model for orbital dynamics 12
4.2.1 Gravitational potential's expansion 13
4.2.2 Non-gravitational forces 14
4.2.3 Relativistic effects 16
4.3 Runge-Kutta method 17
4.4 Spectral analysis 20

5 Dynamical simulations and resultant accelerations **23**
5.1 Operating conditions of simulations 23
5.2 Reference frames 24
5.3 Results of simulations 27
5.3.1 Spring equinox: orbital plane parallel to direction of solar rays 27
5.3.2 Spring equinox: orbital plane perpendicular to direction of solar rays 34
5.3.3 Summer solstice: orbital plane parallel to direction of solar rays 38
5.3.4 Summer solstice: orbital plane perpendicular to direction of solar rays 43
5.4 Results of spectral analysis 49
5.4.1 Spring equinox: orbital plane parallel to direction of solar rays 49
5.4.2 Spring equinox: orbital plane perpendicular to direction of solar rays 51

5.4.3 Summer solstice: orbital plane parallel to direction of solar rays 54
5.4.4 Summer solstice: orbital plane perpendicular to direction of solar rays 55

6 POD: Precise Orbit Determination 59

7 Accelerometer's characteristics 67

8 Conclusions 71

9 Acknowledgement 73

10 Bibliography 75

1 Introduction

A space mission design consists in different phases in which all characteristics of each part of the satellite have to be defined. For scientific missions the choice of the on-board instruments is fundamental to reach the desired goals and it can determine success or failure of the entire work.
METRIC is a proposed mission that will foresee a small satellite placed in an eccentric polar orbit, tracked from ground and space and with an on-board 3-axis accelerometer. It has to measure the non-gravitational accelerations acting on the spacecraft. The accelerometer is considered the payload of the mission because its measurements will be then processed post-flight in order to have a better estimation of some effects of the gravitational physics, of the general relativity and also of the atmospheric density.
In-situ measurements like these of METRIC would represent a step forward in the improvement of the near-Earth environment's knowledge. Therefore it's important to define the accelerometer's characteristics as well as possible.
The goal of this thesis is a preliminary design of a the accelerometer for the METRIC mission, computing the principal features of the instrument: the dynamic range (the interval of accelerations that the accelerometer can measure), the accuracy (how much the single measure differs from the "real" one) and the bandwidth (the band of signal's frequencies in which the instrument collects data).
An orbital simulator based on the known models (of gravitation, atmospheric density, etc.) is implemented in Matlab©. It allows to evaluate the intensity of each contribution measured by the accelerometer in order to estimate the range of the instrument. Then, through a spectral analysis with FFT (Fast Fourier Transform), it is possible to determine the expected frequencies of the acceleration signal and choose the accelerometer's bandwidth.
Concerning the accuracy, it is evaluated considering tracking data. Indeed with SLR (Satellite Laser Tracking), the orbit of the spacecraft, and then also orbital parameters, can be computed making a POD (Precise Orbit Determination). Especially RAAN (Right Ascension of Ascending Node) and AOP (Argument Of Perigee) are interesting for the estimation of general relativity, because removing the non-gravitational accelerations (measured with the accelerometer) and the non spherical contributions of gravity from data of POD it's possible to compute the effects due to only relativity. If the measured data of drag and SRP are precise (i.e. if the accelerometer's accuracy is high), then also the results about the relativistic effects are precise. However the accuracy can't be so high, otherwise it isn't feasible.

Afterwards the designed accelerometer is compared with the existing ones. Accelerometers of past missions, with similar scientific goals (e.g. GRACE, CHAMP), are considered. With this comparison it's also possible to establish the feasibility of the instrument.

2 Missions for near-Earth environment

The near-Earth environment is an important field of study for many years. Nowadays there are several models that try to describe atmospheric density, general relativity or Earth's gravity field, for example. These models are empirical and consist in a series of coefficients that multiply functions of different parameters like latitude, longitude, time,etc. according to the variables that define the desired quantity.
Several space missions were launched to investigate the characteristics of the near-Earth environment and improve the knowledge of it.

2.1 LAGEOS and LARES

In 1976 LAGEOS 1 satellite was launched. It was the first of two satellites of LAGEOS (LAser GEOdynamics Satellite) mission [14][17]. It had several goals: a precise determination of ground stations' position (and consequently the motion of the tectonic plates), the measurement of the Earth's gravity field, the "wobble" of Earth's rotation axis and the estimation, in a more accurate way, of the length of a day.

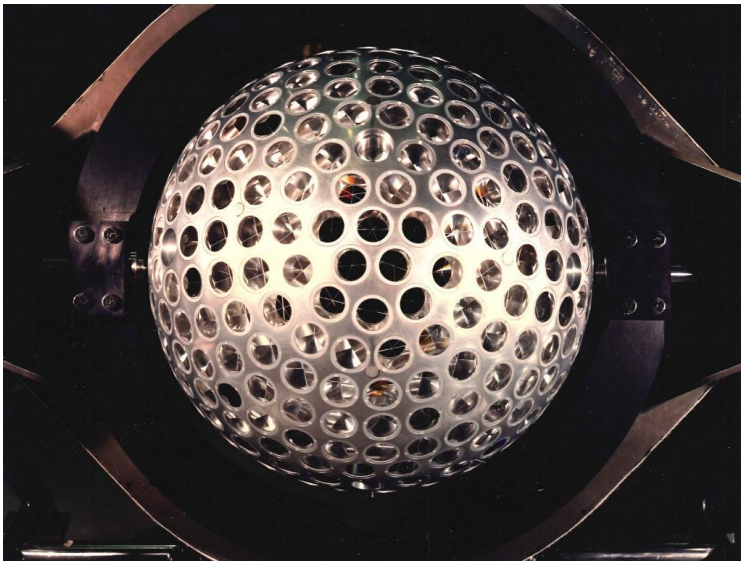

Figure 1: LAGEOS II satellite built by ASI. Credit: ASI

LAGEOS satellites were passive satellites with no power, communications or moving parts. The design of the satellites with lots of corner cube reflectors (Figure 1) allowed to track their position by measuring travel time of laser beams transmitted from ground stations.
For the first time, with this mission, there was the opportunity to obtain laser-

ranging data with high accuracy without errors due to satellite's orbit or array.
Italian mission LARES (LAser Relativity Satellite)[15] is more recent than LAGEOS, but with the same architecture. Two satellites (LARES and LARES 2) have been launched respectively in February 2013 and July 2022. Thanks to their structures, materials and forms, spacecrafts aim to minimize non-gravitational effects as much as possible in order to be influenced only by gravity. This leads to an accurate determination of the Earth's gravitomagnetic field and of the Lense-Thirring effect (a component of relativistic effects) through the analysis of tracking data.

2.2 CHAMP

Another important scientific mission was CHAMP (CHAllenging Minisatellite Payload) [16][10]. It was launched in July 2000 aiming to measure gravity and magnetic field with high accuracy. In particular variations of both fields in both space and time had to be evaluated.
CHAMP's payloads include an accelerometer, magnetometers, a GPS receiver, etc. The accelerometer measured non-gravitational accelerations in order to compute their effects on the orbit, which was determined with the GPS receiver[1] with an high accuracy. In this way non-gravitational effects could be removed leaving only the contributions of purely gravitational perturbations that could be evaluated in order to estimate the Earth's gravity field.

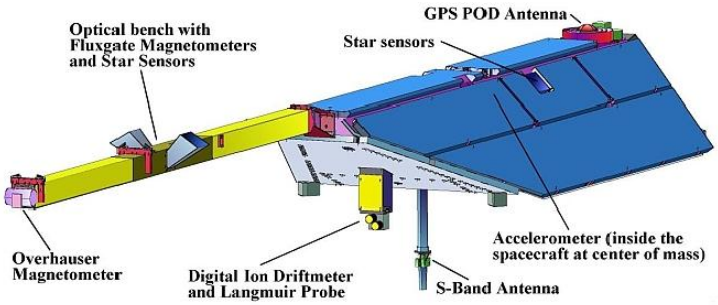

Figure 2: CHAMP spacecraft model. Credit: GFZ

2.3 GRACE

GRACE (Gravity Recovery and Climate Experiment) [12][13] foresaw two satellites (Figure 3) orbiting in LEO orbits, which aimed to collect data about gravity field.

[1]GPS receiver used on CHAMP was the BlackJack of TRSR[5].

The distance between the two satellites was measured with a K-band Ranging System with strong precision. The satellites were in the same orbital plane, but, due to their different positions, they were subjected to different gravitational forces. This leads to variations of the inter-satellite range. Each satellite had high-accuracy accelerometers, which measured non-gravitational accelerations as in CHAMP, and a GPS receiver to determine the position in order to precisely estimate the gravity field models.
GRACE results were also used to study the changes in distribution of mass (both in the oceans, both in the atmosphere and solid Earth).

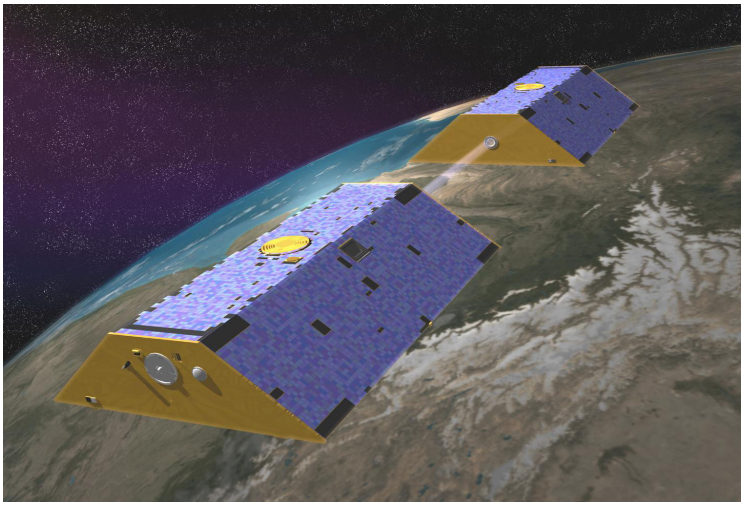

Figure 3: GRACE satellites. Credit: DLR

2.4 GOCE

The last scientific mission mentioned in this thesis is GOCE (Gravity field and steady-state Ocean Circulation Explorer) [11]. The satellite was operational from 2009 to 2013 with the objective of determining the stationary gravitational field, geoid and gravity anomalies with high accuracy.
GOCE provided some interesting components, such as the Electrostatic Gravity Gradiometer (EGG), whose goal was the measurement of the three components of the GGT (Gravity-Gradient Tensor). Satellite foresaw also components that allowed the tracking both from the GPS constellation and from ground, and an Ion Propulsion Assembly which compensated continuously the drag through a thruster in order to have a drag-free satellite.
With these instruments the mission was able to collect, with high spatial resolution

and accuracy, data of the Earth's gravity field and of the geoid, i.e. the equipotential surface of the Earth's gravity field potential.

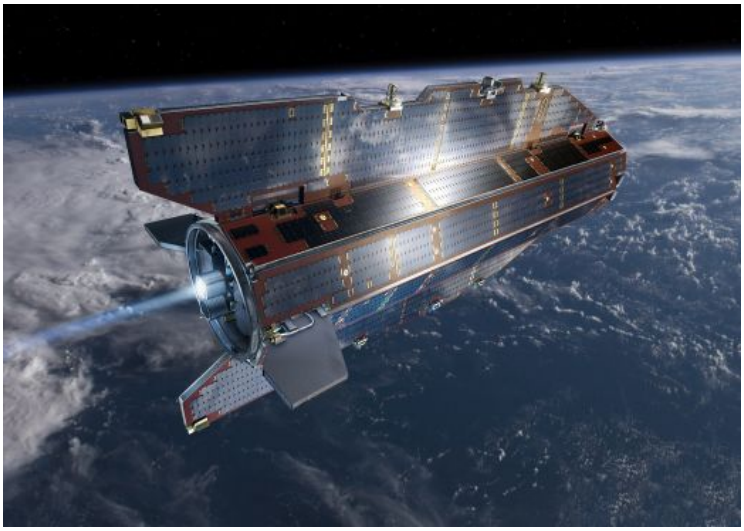

Figure 4: GOCE satellite. Credit: ESA

3 METRIC mission

METRIC (Measurement of EnvironmenTal and Relativistic In-orbit preCessions) [1][6] is a proposed scientific mission that focuses its goals in the study of near-Earth environment's physics and characteristics (atmospheric drag, gravity field, geodesy and general relativity).
Generally, evaluation of the effects of relativity on a test mass around a gravitating body (e.g. a planet like Earth) is based on a platform which is not disturbed by non-gravitational forces. This issue can be dealt with a drag-free (like GOCE) or drag-compensated satellite, which especially requires fine actuators, controlled through the accelerations measured by an on-board accelerometer, in order to cancel or mostly compensate the effects of non-gravitational forces.
However, a virtually drag-free satellite represents a simpler solution to be realized. Indeed it doesn't require a propulsion system to contrast the effects of drag and solar radiation pressure, because the satellite is let orbiting around the gravitating body, affected also by the non-gravitational forces. An accurate 3-axis accelerometer, instead, is needed to measure precisely the disturbing accelerations in order to remove them post flight and then, together with a detailed knowledge of the secular effects of gravity terms, estimate the relativistic contributions.
Regarding density models of the upper atmosphere, they have been obtained through various techniques, such as tracking of satellites, radar sounding of the atmosphere, in-situ pressure measurements. Anyway the models can be further improved, and in-situ measurements of acceleration can represent the next step towards the target. Again, these measurements require an accurate accelerometer, but they are limited to satellites that orbit at low altitudes, where the effect of drag is much higher than that of SRP.
However, an eccentric orbit is considered to increase the orbital lifetime of the satellite. This leads the spacecraft to cover a wider region than that in which the effect of drag is dominating. So a method to separate the contributions of drag and solar radiation pressure is needed.
The architecture and orbit of METRIC are, among the other goals, designed to address these issues.

3.1 METRIC goals

METRIC aims to improve the results obtained by the aforementioned missions taking a cue from them.

In particular, considering also the previous arguments, METRIC's objectives can be summarized as follows:

1. mapping atmospheric density of orbital region of interest;
2. improve the knowledge of selected tidal terms;
3. conduct fundamental physics tests in order to verify the accuracy of the equation of motion due to general relativity;
4. establish a space-based tie among different space geodesy technique.

The first goal requires measurements by an accelerometer so that the accelerations only due to drag can be extracted from them. As above stated, the choice of orbit may simplify the separation between the non-gravitational contributions.
The following two objectives are the reasons for which the satellite has to be considered a test mass. In this case, differently from the previous goal, data obtained by the accelerometer are considered like disturbs for the parameters of interest and will be removed from tracking data in order to estimate at the end the effects of general relativity.
The last objective is related to the spacecraft tracking and system configuration. The main concept is to realize the space counterpart of what is known as a local tie in geodesy by creating a well-known metrological platform that may host various space geodesy techniques.
As previously said, the architecture and the orbit of METRIC must be chosen accurately in order to reach each goal.

3.2 METRIC orbit

Satellite's orbit is a polar eccentric orbit with the apogee at 1200 km of altitude and the perigee at 450 km.
The choice of orbit's characteristics is due to different reasons. The inclination of 90° allows to cancel the even terms in gravity expansion series, which mostly contribute to orbit's perturbation. This leads to have a precession of nodal line only due to non-gravitational forces and not to gravity effects, and then a better analysis of relativistic effects is allowed.
Instead, the eccentricity simplifies the estimation of drag-related accelerations because they can be separated by solar pressure-related ones. Indeed, near the perigee the accelerations due to drag are higher than the ones due to solar radiation pressure, while, at the apogee, the effects of solar pressure are much important than those of drag. The accelerations due to SRP are also quite constant (except if the

satellite goes into eclipse), while the ones related to drag change a lot during an orbital period.

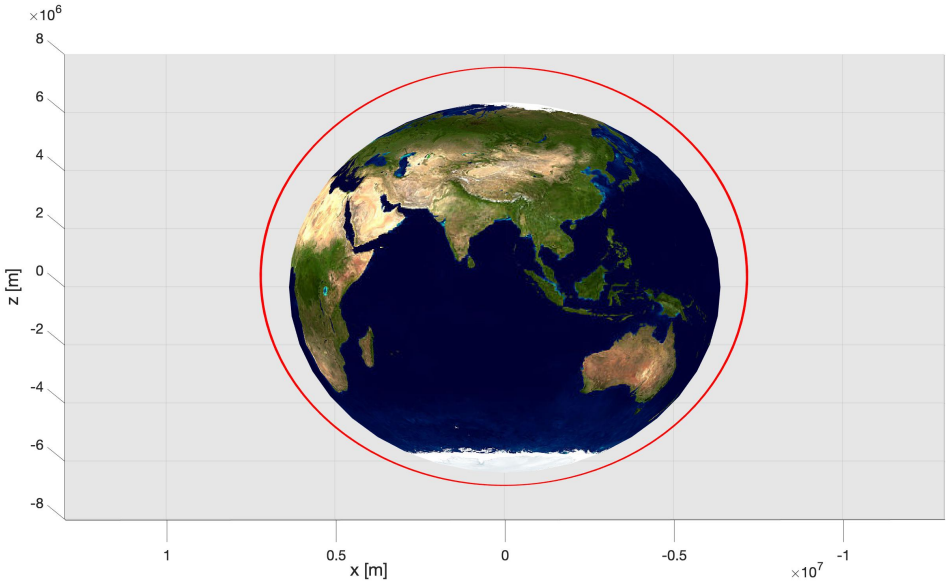

Figure 5: METRIC's eccentric orbit.

3.3 Satellite and on-board instruments

Satellite's design foresees a small sphere with radius of 30 cm and laser retroreflectors on the surface. The expected mass of the satellite is 100 kg. The spherical form leads as consequence that the cross section is constant for both solar radiation pressure and drag, so it's simpler to compute their effects in post-processing, because it is not necessary to evaluate spaceraft's attitude.

However an attitude and determination system is expected. It includes, in particular, magnetorquers, which has to guarantee a spin of the satellite so that the accelerations measured by a precise accelerometer can be modulated. In this way also constant contributions (constant in absolute value) appear as oscillating signals with zero average. So the spin allows to simplify the separation of measured accelerations.

As just mentioned, also an accelerometer has to be mounted on-board the satellite. It is fundamental for the achievement of mission's goals, so its design and characteristics have to be chosen as well as possible. The accelerometer measures the non-gravitational accelerations acting on spacecraft. Accelerations must be evaluated in space, so a 3-axis accelerometer is needed. Its expected characteristics, and how to determine them, are better explain in the following Chapters.

The last component of METRIC's instrumentation is a GPS receiver. It allows tracking of the spacecraft from space (with GNSS), while the retroreflectors on the surface allow, on the other side, the tracking from ground (SLR). Combining the two techniques, the position of the satellite can be known continuously, leading to a precise orbit determination. Also orbital parameters, especially the rotation of both the nodal line and perigee, can be estimated in order to evaluate the effects of general relativity post-flight.
Anyway, all the components must be placed in order to reduce oscillations and vibrations. These would excite the accelerometer with noising signals and compromise the measurements.

4 Dynamical model

The determination of accelerometer's characteristics passes through simulations of the accelerations that the satellite is expected to undergo. So it becomes necessary to use a dynamical model as precise as possible. It has to include all gravitational and non-gravitational forces that will be studied (Earth's gravity model, drag, solar radiation pressure) and relativistic effects.
Furthermore the accuracy must be at least of the lowest order of magnitude of the accelerations considered. In particular, it's known from literature that the expected orders of magnitude of non-gravitational accelerations (their contributions are much smaller than those of gravity) are between 10^{-10} and 10^{-7} m/s^2 for drag-related ones, 10^{-9} and 10^{-8} m/s^2 for accelerations due to SRP and between 10^{-10} and 10^{-8} m/s^2 for relativistic ones. So the simulator must resolve accelerations lower than 10^{-10} m/s^2 in order to have also a safety margin in the estimation of all effects.

4.1 Software: Matlab© & GMAT

To simulate the dynamics of the satellite two software have been considered for this thesis.
The first one is GMAT (General Mission Analysis Tool)[2]. It is an open source tool developed by NASA that allows to simulate space missions.
The user can set the orbit parameters (both in Cartesian or Keplerian coordinates, for example), the duration of simulation and the characteristics of the spacecraft. Moreover, it's possible to configure the numerical integrator. In particular the most important values[3] that can be set are:

- numerical method: defining which mathematical method is used for the integration (default method is RungeKutta89);
- accuracy: for each step the integrator ensures that the error is lower than the set value;
- step size: step size can vary between two values (MaxStep e MinStep) in order to respect the accuracy in a certain number of attempts (MaxStepAttempts).

Another field of interest for the configuration of the simulator is the ForceModel. In this field it is possible to choose which forces act on the satellite, the reference

[2] https://software.nasa.gov/software/GSC-17177-1
[3] A complete guide is presented in [3].

models for them (e.g. MSISE or Jacchia Roberts for atmosphere) and both the model and the order of series expansion for the gravity.
Graphics, ground tracking, data files can be obtained as results of the simulations. However since the requested accuracy is remarkable, the computational costs are too expensive for GMAT so it's not reliable for the objectives of the thesis.
The second software considered is Matlab© (MATrix LABoratory)[4] by MathWorks. It is a programming language that allows to implement mathematical algorithms through matrix calculation. Also because of the possibility to exploit several Toolboxes[5], Matlab© is very flexible and can be used for every field that requires computation.
A cons of Matlab© with respect to GMAT is that the simulator must be implemented starting from zero. However Matlab© allows to reduce the computation time reaching the requested accuracy (this has been confirmed with some tests).

4.2 Mathematical model for orbital dynamics

The motion of the satellite can be influenced by different forces: gravitational forces of the planet around which the satellite is, non-gravitational such as drag and solar radiation pressure. Then also relativistic corrections are important due to the high velocity of the satellite. All these effects have to be taken into account in the dynamical model.
Starting from the two body problem [8], in order to simplify the model and the computation, it is possible to write the following equation of motion:

$$\ddot{\mathbf{r}} = -\frac{\mu}{r^3}\mathbf{r} + \mathbf{p} \tag{1}$$

where $\mathbf{r}$ is the position vector (r its norm), μ is the planet's gravitational constant and $\mathbf{p}$ can be considered as a disturbing acceleration.
The first term of the equation is the spherical term of the gravitational potential of the planet and represents the effect of gravity due to an idealized perfect spherical body. Instead, the second term can involve different contributions based on which kind of effects are studied or how accurate the model is (the more contributions are considered, the more precise the model is). Since METRIC aims to evaluate both non-gravitational and relativistic effects, the accelerations related to these factors

[4] https://www.mathworks.com/products/matlab.html
[5] A Toolbox contains functions or script files ready to be used.

must be included.

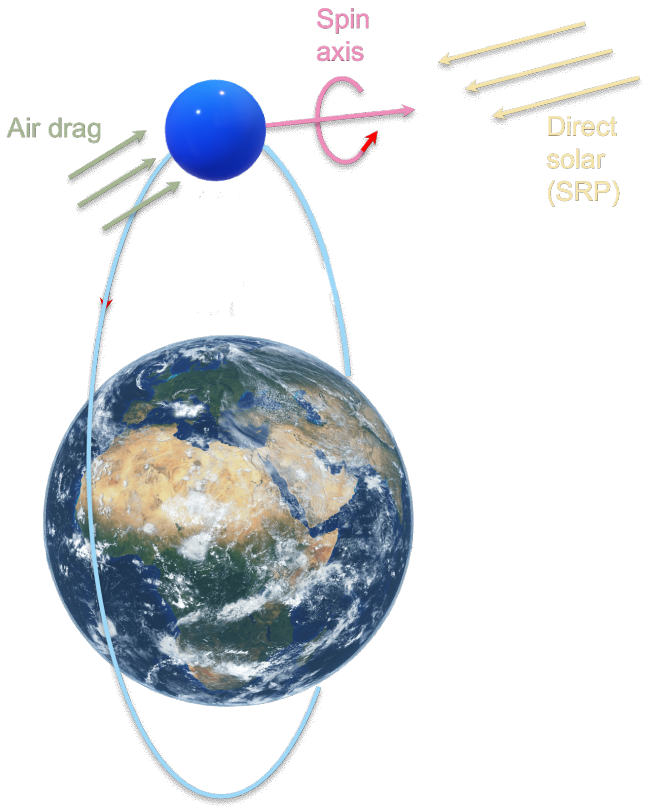

Figure 6: METRIC and acting forces on the satellite. Credit: METRIC

Then, also the non homogeneity of the gravity field produces some important perturbations with respect to the idealized spherical body, so this contribution must be considered too.

4.2.1 Gravitational potential's expansion

Because of the distribution of masses and Earth's oblatness, the gravity field isn't homogeneous. It can be modeled with a series of terms (harmonics) with decreasing amplitude, added to the spherical one. The effects of these terms is smaller than those of the spherical term, so they can be considered as disturbs and included in the perturbation term $\mathbf{p}$.
In particular, in this work, only the first two harmonics are considered, in order to simplify the implementation and also because their effects are the most significant in the perturbation of orbital parameters. These harmonics are related to two zonal coefficients (J_2 and J_3), whose values are reported in Table 1.

Coefficient	Value
J_2	$1.0826 \cdot 10^{-3}$
J_3	$-2.5324 \cdot 10^{-6}$

Table 1: Zonal coefficients values.

The effects of the harmonics can be expressed as accelerations with respect to ECI frame through the Lagrange formulation [7]:

$$\mathbf{a}_{J_2} = -\frac{3}{2} J_2 \mu \frac{R_\oplus^2}{r^5} \left[\left(1 - 5\frac{z^2}{r^2} \right) (x\hat{\mathbf{I}} + y\hat{\mathbf{J}}) + \left(3 - 5\frac{z^2}{r^2} \right) z\hat{\mathbf{K}} \right] \tag{2}$$

$$\mathbf{a}_{J_3} = -\frac{5}{2} J_3 \mu \frac{R_\oplus^3}{r^7} \left[\left(3z - 7\frac{z^3}{r^2} \right) (x\hat{\mathbf{I}} + y\hat{\mathbf{J}}) + \left(6z^2 - -7\frac{z^4}{r^2} - \frac{3}{5} r^2 \right) \hat{\mathbf{K}} \right] \tag{3}$$

$\mathbf{a}_{J_2}$ and $\mathbf{a}_{J_3}$ are respectively the accelerations related to the coefficient J_2 and J_3. The other terms of the equations are:

- $R_\oplus$: Earth's equatorial radius (6378137 m);
- x, y, z: coordinates of position vector expressed in meters;
- $\hat{\mathbf{I}}, \hat{\mathbf{J}}, \hat{\mathbf{K}}$: versors of ECI reference frame.

These accelerations generally cause a rotation of nodal line and periapsis. However, as aforementioned, METRIC's RAAN isn't influenced by non-spherical effects, because of the orbital inclination which allows to cancel the even terms of gravity expansion, i.e. J_2 (effects due to J_3 on RAAN are quite small).

4.2.2 Non-gravitational forces

Another contribution that must be considered in the perturbation term is the effect of non-gravitational forces: drag and solar radiation pressure.
Drag is the resistance of atmosphere's particles. As aforementioned, due to the choice of orbit, the drag is important near the perigee and decreases near the apogee because the atmosphere at that altitude (1200 km) is very rarefied.
The drag-related acceleration can be expressed as:

$$\mathbf{a}_{drag} = \frac{1}{2} \rho v \frac{A}{m} C_D \mathbf{v}_{rel} \tag{4}$$

in which ρ is the atmosphere's density, $\mathbf{v}_{rel}$ is the vector of spacecraft's velocity relative to the atmosphere (v is its norm), A is the cross-section, m is the satellite's

mass and C_D is the drag coefficient.
C_D is assumed constant in order to simplify the problem with a value of $C_D = 2.2$ which is a typical mean value for this kind of applications. The cross-section is constant too, because of the satellite's geometry. The spherical shape leads to a circular cross-section area and so its value can be computed as $A = \pi r^2$ (r radius of the satellite).
In the end, the atmosphere's density ρ depends on the spacecraft's position in the atmosphere, and it can be computed from known models. Currently there are several empirical models that describe with a good approximation the density of the atmosphere. One of this is the NRLMSISE-00, which is used in the building of the simulator because Matlab© provides a function that implements this model. The function is called *atmosnrlmsise00*[6] and wants in input the spherical coordinates (latitude, longitude and height) of the evaluation point and the precise moment of the year in which computing the atmosphere's characteristics. Function returns as outputs the temperature and the density of the selected atmosphere's point at the input time.
Both the position and the evaluation time are important for the atmosphere's density, because it varies both in space and time as it is influenced by solar activity.

The other non-gravitational force considered is the solar radiation pressure (SRP). It is the force per unit area that solar photons exert on the spacecraft. The acceleration due to SRP is:

$$\mathbf{a}_{srp} = \nu C_r \frac{A}{m} P_0 \frac{\mathbf{r}_\odot}{r_\odot} \tag{5}$$

where ν is a coefficient related to eclipses, C_r is the reflectivity of the spacecraft, P_0 is the solar pressure per unit area at distance of 1 AU ($4.56 \cdot 10^{-6}$ N/m^2), $\mathbf{r}_\odot$ is the position vector of the satellite with respect to Sun ($r_\odot$ is its norm).
The ν coefficient is obtained with a function that evaluates if the Sun is visible by the spacecraft or overshadowed by Earth or Moon through geometrical considerations. The value of ν is 1 when the Sun is visible and so the solar radiation pressure acts on the satellite, while $\nu = 0$ when the satellite is in Umbra, so that photons can't reach the spacecraft. For simplicity the effect of albedo isn't considered.
The reflectivity of the satellite depends on the surface material, but it is not yet known, so the value of C_r is set to a typical value of 1.8.
Also in this case the cross-section area is constant due to the spacecraft's geometry.

[6]The complete documentation about the function can be found on https://www.mathworks.com/help/aerotbx/ug/atmosnrlmsise00.html

4.2.3 Relativistic effects

Following the IERS (International Earth Rotation and Reference System Service) Convention (2010) the relativistic acceleration that must be added to correct the dynamical model can be divided in three contributions: gravitoelectric, gravitomagnetic and geodetic. All these terms are quite small (orders of magnitude between 10^{-12} and 10^{-9} m/s^2) and so they are considered disturbs with respect to the effects of spherical gravitational term.
The formulation of the relativistic accelerations can be expressed, as presented in [6], as:

$$\begin{aligned}\mathbf{a}_{rel} = \frac{GM_\oplus}{c^2 r^3}\Bigg\{\left[2(\beta+\gamma)\frac{GM_\oplus}{r} - \gamma\dot{\mathbf{r}}\cdot\dot{\mathbf{r}}\right]\mathbf{r} + 2(1+\gamma)(\mathbf{r}\cdot\dot{\mathbf{r}})\dot{\mathbf{r}}\Bigg\} + \\ (1+\gamma)\frac{GM_\oplus}{c^2 r^3}\left[\frac{3}{r^2}(\mathbf{r}\times\dot{\mathbf{r}})(\mathbf{r}\cdot\mathbf{J}_\oplus) + (\dot{\mathbf{r}}\times\mathbf{J}_\oplus)\right] + \\ \left\{(1+2\gamma)\left[\dot{\mathbf{R}}\times\left(\frac{GM_\odot\mathbf{R}}{c^2R^3}\right)\right]\times\dot{\mathbf{r}}\right\}\end{aligned} \tag{6}$$

in which $GM_\oplus$ and $GM_\odot$ are the gravitational coefficients of Earth and Sun respectively, c is the speed of light, β and γ are PPN (parameterized post-Newtonian), $J_\oplus$ is the Earth's angular momentum per unit mass and $\mathbf{R}$ is the position vector of the Earth with respect to Sun (R is its absolute value).
β and γ are set equal to 1 with good approximation because, also through different missions and experiments about general relativity, it has been demonstrated that $\beta - 1 \sim 8\cdot10^{-5}$ and $\gamma - 1 \sim 2.3\cdot10^{-5}$. The Earth's angular momentum per unit mass is a vector defined as $J_\oplus = [0\ 0\ \frac{2}{5}R_\oplus^2\omega_e]^T$, assuming, for simplicity, that the Earth is a perfect spherical body, with ω_e the rotational velocity of the Earth.
As above stated, the acceleration due to relativistic effects can be divided in three terms. The first one in Equation (6) is also called Schwarzschild term and it's the dominant contribution between the relativistic effects. It influences in particular the rotation of the perigee. The second term is called Lense-Thirring term, it's one or two orders of magnitude smaller than Schwarzschild one and acts on the precession of nodal line. The last term, De Sitter term, is the less intense effect.
Anyway all these effects are small, as aforementioned, leading to accelerations of low orders of magnitude. Moreover the results of rotation of nodal line or perigee due to relativity are in the order of $arcsec/year$.

In conclusion, after the discussion of each perturbing contribution, it's possible to establish which is the second term that must be considered in Equation (1):

$$\mathbf{p} = \mathbf{a}_{J_2} + \mathbf{a}_{J_3} + \mathbf{a}_{drag} + \mathbf{a}_{srp} + \mathbf{a}_{rel} \tag{7}$$

In this way the mathematical model is completed. However it is based on a second order differential equation, so a numerical integrator is needed. The numerical integrator chosen and implemented is a Runge-Kutta method of fourth order.

4.3 Runge-Kutta method

Runge-Kutta methods are some of the most used methods for numerical integration. The idea of every RK method is to evaluate the space vector $\mathbf{y}_{i+1}$ at time $t_{i+1} = t_i + h$, where h is the integration step, adding an increment to the previous state vector $\mathbf{y}_i$.

$$\mathbf{y}_{i+1} = \mathbf{y}_i + h\phi(t_i, \mathbf{y}_i, h) \tag{8}$$

$\phi(t_i, \mathbf{y}_i, h)$ is the increment function and depends on the first derivative of $\mathbf{y}$ evaluated over the interval $[t_i, t_i + h]$. The order (if less than the 5th) of Runge-Kutta method is equal to the number of evaluation points (or stages) in which the function is computed between t_i and $t_i + h$. Increasing the order, the number of stages increases and so also the accuracy of integration.
The first derivative function $\mathbf{f}(t, \mathbf{y})$ is not known explicitly, but it can be obtained from the differential Equation of motion (1). As aforementioned it is a second order differential equation and so represents the second derivative. However it can be rearranged as a system of first order differential equations, assuming that $\mathbf{v} = \dot{\mathbf{r}}$ (velocity is the first derivative of position) and $\mathbf{a} = \ddot{\mathbf{r}} = \dot{\mathbf{v}}$ (acceleration is the first derivative of velocity). In this way if the state vector $\mathbf{y}$ is considered as:

$$\mathbf{y} = \Big\{ r_x, \quad v_x, \quad r_y, \quad v_y, \quad r_z, \quad v_z \Big\} \tag{9}$$

and the equation of motion can be written as follows:

$$\begin{cases} \dot{y}_1 = y_2 \\ \dot{y}_2 = -\frac{\mu}{r^3} y_1 + p_x \\ \dot{y}_3 = y_4 \\ \dot{y}_4 = -\frac{\mu}{r^3} y_3 + p_y \\ \dot{y}_5 = y_6 \\ \dot{y}_6 = -\frac{\mu}{r^3} y_5 + p_z \end{cases} \tag{10}$$

where y_i indicates the i-th component of the state vector. Knowing that $\dot{\mathbf{y}} = \mathbf{f}(t, \mathbf{y})$, the derivative function is:

$$\mathbf{f}(t, \mathbf{y}) = \begin{Bmatrix} y_2 \\ -\frac{\mu}{r^3} y_1 + p_x \\ y_4 \\ -\frac{\mu}{r^3} y_3 + p_y \\ y_6 \\ -\frac{\mu}{r^3} y_5 + p_z \end{Bmatrix} \tag{11}$$

In this work a Runge-Kutta method of fourth order has been chosen, because it is one of the most common and it is also relatively simple to implement. There are four evaluation times $\tilde{t}$ and each one is obtained from

$$\tilde{t}_m = t_i + a_m h, \qquad m = 1, 2, 3, 4 \tag{12}$$

At every time the value of the state vector $\tilde{\mathbf{y}}$ can be computed through

$$\tilde{\mathbf{y}}_m = \mathbf{y}_i + h \sum_{n=1}^{m-1} b_{mn} \mathbf{f}_n, \qquad m = 1, 2, 3, 4 \tag{13}$$

while the derivatives vector is evaluated substituting $\tilde{t}_m$ and $\tilde{\mathbf{y}}_m$ in Equation (11),

$$\tilde{\mathbf{f}}_m = \tilde{\mathbf{f}}(\tilde{t}_m, \tilde{\mathbf{y}}_m), \qquad m = 1, 2, 3, 4 \tag{14}$$

The increment function takes into account a weight c_m for each evaluation point and its equation is

$$\phi = \sum_{m=1}^{4} c_m \tilde{\mathbf{f}}_m \tag{15}$$

Substituting all the informations in Equation (8) it's possible to obtain

$$\mathbf{y}_{i+1} = \mathbf{y}_i + h \sum_{m=1}^{4} c_m \tilde{\mathbf{f}}_m \tag{16}$$

The coefficients a_m, b_{mn} and c_m for a fourth order Runge-Kutta method are:

$$[\mathbf{a}] = \begin{Bmatrix} 0 \\ 1/2 \\ 1/2 \\ 1 \end{Bmatrix} \qquad [\mathbf{b}] = \begin{Bmatrix} 0 & 0 & 0 \\ 1/2 & 0 & 0 \\ 0 & 1/2 & 0 \\ 0 & 0 & 1 \end{Bmatrix} \qquad [\mathbf{c}] = \begin{Bmatrix} 1/6 \\ 1/3 \\ 1/3 \\ 1/6 \end{Bmatrix}$$

In conclusion, the algorithm to implement is:

$\tilde{\mathbf{f}}_1 = \mathbf{f}(t_i, \mathbf{y}_i)$

$\tilde{\mathbf{f}}_2 = \mathbf{f}(t_i + \frac{1}{2}h, \mathbf{y}_i + \frac{1}{2}h\tilde{\mathbf{f}}_1)$

$\tilde{\mathbf{f}}_3 = \mathbf{f}(t_i + \frac{1}{2}h, \mathbf{y}_i + \frac{1}{2}h\tilde{\mathbf{f}}_2)$

$\tilde{\mathbf{f}}_4 = \mathbf{f}(t_i + h, \mathbf{y}_i + h\tilde{\mathbf{f}}_3)$

$\mathbf{y}_{i+1} = \mathbf{y}_i + h\left(\frac{1}{6}\tilde{\mathbf{f}}_1 + \frac{1}{3}\tilde{\mathbf{f}}_2 + \frac{1}{3}\tilde{\mathbf{f}}_3 + \frac{1}{6}\tilde{\mathbf{f}}_4\right)$

However a differential equation can have infinite solutions, but if initial boundary conditions are set, the solution is unique.
For the equation of motion of the spacecraft, a first state vector must be set, indicating the initial position and velocity of the satellite, which depend on the orbit that has to be studied. From those values, the integrator evaluates the following state vector (position and velocity after the integration step) and so on.
In this way the orbit can be reconstructed through a series of consecutive points and for each point it's possible to know the accelerations due to all implemented effects

(they can be obtained from the functions that simulate respectively drag, SRP and relativistic effects when the perturbation term has to be computed).
The accelerations are ideally measured by the accelerometer and then analyzed in post processing. The analysis includes both an analysis in term of intensity of each acceleration and a spectral analysis in order to study the band of frequencies in which each contribution acts.

4.4 Spectral analysis

The last part which concerns with the evaluation of accelerations acting on satellite is the spectral analysis. This allows to know the behaviour of accelerations in terms of frequency, and so how fast they oscillate or change in time. This is important because the accelerometer can accurately measure only accelerations that changes with a frequency included into a fixed band.
Spectral analysis can be implemented with different methods. The fast Fourier transform (FFT) is the method chosen for this thesis because it is one of the most used and also because it is already implemented in Matlab©. The function *fft*[7] computes the discrete Fourier transform (DFT) of a signal through the FFT algorithm. In general the Fourier transform is a mathematical operator that associates a function in time domain $x(t)$ to a function in frequency domain $X(f)$ as follows:

$$X(f) = \int_{-\infty}^{+\infty} x(t) e^{-j2\pi ft} dt \tag{17}$$

However if the data available are not continuous but discrete (as for all measurement tools that acquire data with a finite sampling frequency) the Fourier transform is modified into a discrete transform (DFT):

$$X_k = \sum_{i=0}^{N-1} x_i e^{-\frac{j2\pi ki}{N}} \qquad k = 0, 1, 2, ..., N-1 \tag{18}$$

where N is the number of samples acquired and available.
The fast Fourier transform is based on the discrete Fourier transform, but has a slightly different algorithm which is computationally faster than the normal DFT. With this operator, the signal that has to be analyzed is decomposed in a sum of sines and cosines with different amplitudes and frequencies. Indeed the exponential

[7] Function's documentation is available on https://www.mathworks.com/help/matlab/ref/fft.html

term in Equation (18) can be written through Euler's formula[8] as:

$$e^{-\frac{j2\pi ki}{N}} = cos\left(\frac{2\pi ki}{N}\right) - jsin\left(\frac{2\pi ki}{N}\right) \tag{19}$$

Then the power spectral density (PSD) is computed in order to evaluate better the distribution of signal frequency components. It represents the contribution in term of power of each frequency component. The PSD is evaluated computing the absolute value of each Fourier transform's term divided by the number of samples.

$$PSD_k = \frac{2}{N}\sqrt{[Re(X_k)]^2 + [Im(X_k)]^2} \tag{20}$$

The 2 at the numerator is due to the fact that the Fourier transform returns both positive and negative frequencies in the interval $[-f_s/2,\ f_s/2]$, where f_s is the sampling frequency. So the two parts of DFT (which are equal in amplitude) are summed.
The PSD obtained gives the informations about which are the most important frequency components of the signal analyzed and their amplitudes. In particular the PSD can have some peaks that represent the components with higher amplitude and so the most significant for the signal. The frequencies of these peaks are then the fundamental frequencies at which the signal propagates.

[8] $e^{j\theta} = cos\theta + jsin\theta$

5 Dynamical simulations and resultant accelerations

The implemented dynamical simulator allows to study several kind of missions. However there is a constraint: the satellite must be around the Earth, because all the models for each contribution in the perturbation term are based on own values of the Earth.
Anyway, respecting this constraint, it's also possible to evaluate the same mission (e.g. METRIC) in different operating conditions, varying some orbital parameters.

5.1 Operating conditions of simulations

Four conditions for METRIC spacecraft are considered: two moments of the year (spring equinox and summer solstice) and for both of them two different orientations of orbital plane with respect to the plane defined by solar rays. The orbital plane is, for the first case, parallel to solar rays' plane (like in Figure 7) and perpendicular in the second condition (like in Figure 8).
Therefore, in summary, the studied cases are:

- Spring equinox with orbital plane parallel to the plane containing solar rays;
- Spring equinox with orbital plane perpendicular to the plane containing solar rays;
- Summer solstice with orbital plane parallel to the plane containing solar rays;
- Summer solstice with orbital plane perpendicular to the plane containing solar rays.

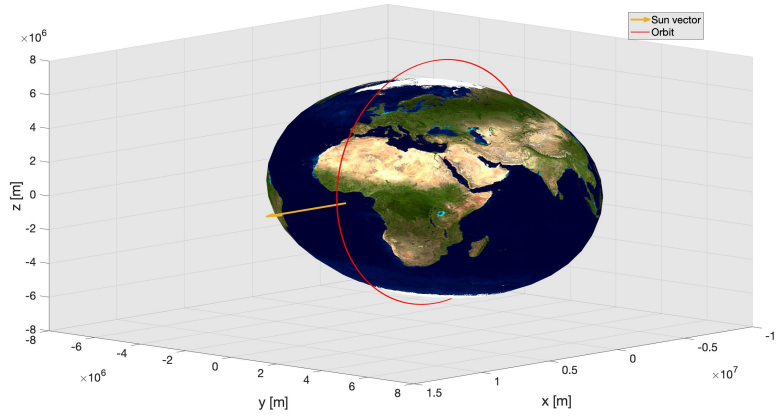

Figure 7: Orbital plane is parallel to the solar rays' direction (in this case the simulation is done at spring equinox).

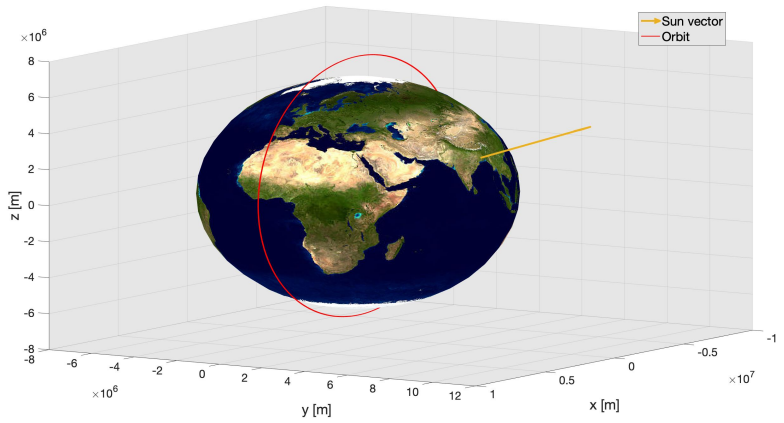

Figure 8: Orbital plane is perpendicular to the solar rays' plane (in this case the simulation is done at summer solstice).

Studying different situations allows to compare, at the end, the effects of non-gravitational and relativistic accelerations in different conditions. In this way it's possible to have a "complete" idea of the physical environment the satellite will undergo and so the choice of accelerometer's characteristics is more detailed and precise because it considers all variables.
Every simulation has a duration of two days (starting from 00:00:00 of 20 March 2023 for cases at spring equinox and from 00:00:00 of 21 June 2023 for summer solstice's cases) with an integration step of 60 seconds. These choices are done in order to not increase too much the computation time, but, at the same time to reach reasonable results, which are described later.

5.2 Reference frames

The reference frame used in the dynamical simulator is ECI (Earth Centered Inertial), which is a geocentric fixed (not rotating with the Earth) system. The x-axis points in the vernal equinox direction and the x-y plane is the Earth's equatorial plane. The z-axis coincides with the Earth's axis of rotation and points northward. All vectors (positions, velocities and accelerations) obtained from the simulator are expressed in ECI reference frame.
However the accelerometer has an own reference system, which is different from ECI because the instrument is mounted inside the spacecraft and so is not fixed but moves with the satellite.
Since this work focuses about the research of accelerometer's characteristics, a ref-

erence frame centered on the satellite's center of mass is needed. The LVLH (Local Vertical-Local Horizontal) is the system chosen. It is based on the local vertical, i.e. the straight line that links the center of the Earth and the spacecraft's center of mass, and on the local horizon, that is the tangent plane to the orbit in the position occupied by the satellite. So, while ECI is fixed, LVLH changes in time due to the motion of the satellite.
LVLH system is defined with:

- the x-axis that lies on the local vertical direction and points towards the zenith;
- the y-axis that is on the local horizon and points in the flight direction;
- the z-axis completes the triad (its direction is normal to orbital plane and parallel to the angular momentum of orbit).

Both ECI and LVLH are shown in Figure 9.

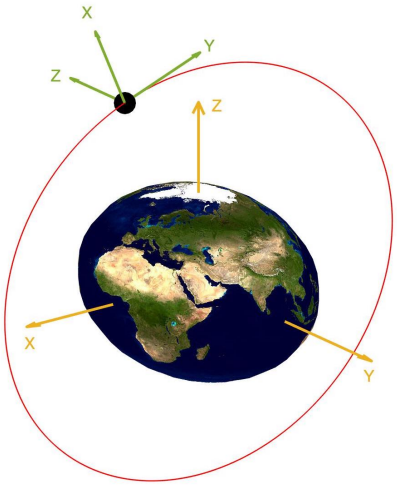

Figure 9: Reference systems: ECI (yellow) and LVLH (green).

As above stated, the vectors obtained from the dynamics have the components aligned with ECI reference system, but especially accelerations are required to be expressed in LVLH. So a rotation matrix is needed in order to perform this transformation.
To compute this matrix it's easier to start from the rotation matrix from LVLH to ECI (which represents the inverse needed transformation), because it's simpler to obtain geometrically. $M_{LVLH \to ECI}$ has the columns that are the versors of LVLH system expressed in ECI. The zenith versor and the angular momentum of orbit must be computed at every step to determine LVLH reference system and also the rotation matrix. The first versor can be calculated starting from the position vector

(that connects the centers of Earth and satellite) at the current time. Dividing the position vector by its norm it's possible to obtain the zenith versor ($\hat{\mathbf{r}}$). The angular momentum's versor, instead, is estimated from both current position and velocity of the satellite. By definition [8], the specific angular momentum[9] is $\mathbf{h} = \mathbf{r} \times \dot{\mathbf{r}}$, so its versor can be computed as:

$$\hat{\mathbf{h}} = \frac{\mathbf{r} \times \dot{\mathbf{r}}}{|\mathbf{r}|\,|\dot{\mathbf{r}}|} \tag{21}$$

with $\dot{\mathbf{r}}$ that is the velocity of the satellite.
The last versor must be orthogonal with respect to both zenith versor and normal versor to orbital plane, so it can be computed as the cross product of the other two. Therefore the rotation matrix from LVLH to ECI can be defined as:

$$M_{LVLH \to ECI} = \left[\hat{\mathbf{r}},\ \hat{\mathbf{h}} \times \hat{\mathbf{r}},\ \hat{\mathbf{h}}\right] \tag{22}$$

The inverse transformation, i.e. from ECI to LVLH (the required transformation), is represented by the inverse matrix of $M_{LVLH \to ECI}$. Because of the properties of rotation matrices, which are orthogonal, the inverse matrix corresponds to the transpose. So the rotation matrix from ECI to LVLH is:

$$M_{ECI \to LVLH} = M^{-1}_{LVLH \to ECI} = M^{T}_{LVLH \to ECI} = \left[\hat{\mathbf{r}},\ \hat{\mathbf{h}} \times \hat{\mathbf{r}},\ \hat{\mathbf{h}}\right]^T \tag{23}$$

As aforementioned, LVLH reference frame isn't fixed and changes in time, so also the rotation matrix varies and it must be computed at each step of integration (i.e. at each position occupied by the satellite).
Through $M_{ECI \to LVLH}$ the accelerations expressed in ECI can be then transformed in LVLH multiplying the rotation matrix and the acceleration vector relative to the same instant of evaluation

$$\{\mathbf{a}_{i,LVLH}\}^T = [M_{i,ECI \to LVLH}]\,\{\mathbf{a}_{i,ECI}\}^T \tag{24}$$

where the subscript i indicates the i-th step of integration.
All accelerations (drag, SRP and relativistic) are rotated from ECI to LVLH in order to be expressed in a reference frame based on the satellite and the accelerometer, so as to simulate the "real" accelerations that accelerometer measures (only non-gravitational) and returns as outputs and then compare them with the relativistic ones in a coherent way. Moreover, for simplicity an intrinsic random noise of the accelerometer isn't considered.

[9] Specific angular momentum is the angular momentum per unit mass.

To be more precise, also the spin of the satellite should be included and so another rotation matrix should be computed in order to pass from LVLH to the own accelerometer reference frame. However, the spin of the spacecraft isn't taken into account in the implemented code because it doesn't change the amplitude and the periodicity of accelerations, but it only makes accelerations being modulated differently, especially constant accelerations which become oscillating. So the spin doesn't influence the determination of instrument's characteristics.
With the simulated measured data it's now possible to think about how to define the required characteristics of the accelerometer in order to reach the goals of the mission.

5.3 Results of simulations

In this paragraph the results of each simulation's case are presented with a series of figures that show the non-gravitational and the relativistic accelerations as functions of time. The first ones could be considered as the outputs of accelerometer and the starting point of data analysis, while the effects of relativity are computed to understand which is the intensity of their contribution.
Drag, solar radiation pressure and relativistic corrections are similar as order of magnitude and represent the lower terms of the perturbing acceleration $\mathbf{p}$ (the accelerations due zonal coefficients of gravity are much higher), so that they are compared one to each others in order to understand which contribution influence more the motion of the satellite on each axis and consequently the orbital parameters.

5.3.1 Spring equinox: orbital plane parallel to direction of solar rays

Each simulation differs from the others because of the operational conditions. The initial state vector must be varied in order to change the situation.
In this case the simulations covers two days from midnight of 20 March 2023 to midnight of 22 March 2023. As it's at spring equinox, the Sun is on the vernal direction, so on x-axis of ECI reference system. This leads that, if the orbital plane has to be parallel to solar rays' direction, it must lie on x-z plane (remember that the orbit is a polar orbit).
This argument brings to define the initial state vector assuming that the simulation starts when the satellite is at the perigee.

$$\mathbf{y}_0 = \Big\{0, \quad 7.837 \cdot 10^3, \quad 0, \quad 0, \quad -6.828 \cdot 10^6, \quad 0\Big\}$$

The position's components are expressed in m while the velocity's components in m/s^2.
Supposing that the argument of perigee is 270°, the nearest point to Earth is on the negative part of z-axis at an altitude of 450 km (as the orbit is defined) and the velocity has only the x component, because it is tangential to orbit at the apsidal points and, as above stated, the orbital plane is on the x-z plane.
Furthermore, in order to define the value of velocity, the energy law for elliptical orbits [8] is used

$$\frac{v^2}{2} - \frac{\mu}{r} = \frac{\mu}{2a} \tag{25}$$

where the semi-major axis can be computed as the mean of perigee and apogee: $a = (r_a + r_p)/2$. Rearranging Equation (25), the velocity at the perigee is:

$$v = \sqrt{\frac{2\mu}{r_p} + \frac{\mu}{a}} \tag{26}$$

It represents the second term in the state vector (velocity along x-axis).
Once defined the initial conditions for the numerical integrator the simulation can start. Only non-gravitational accelerations and relativistic corrections are presented as results, because they're the important data for instrument's characteristics definition: drag and SRP because they are the measured contributions, relativistic ones because they are important for the study of general relativity (a goal of the mission) and allow to estimate the accuracy through some considerations which are better explained later.

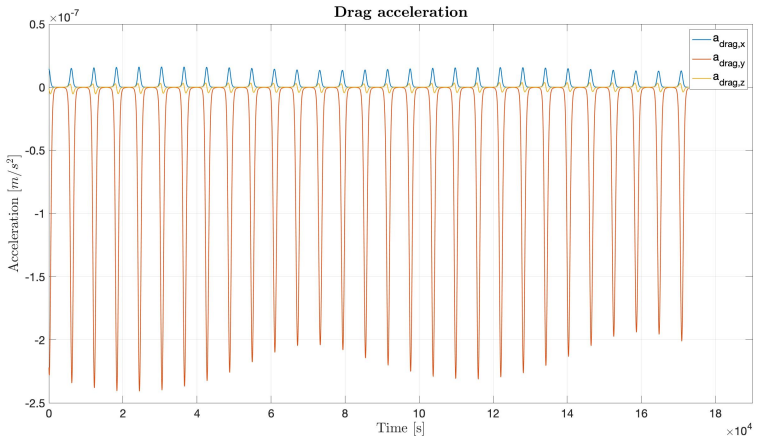

Figure 10: Drag-related acceleration in LVLH reference system

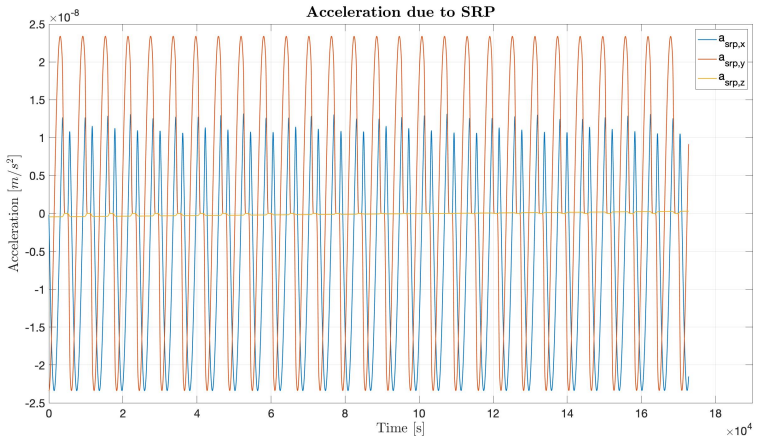

Figure 11: Acceleration due to SRP in LVLH reference system

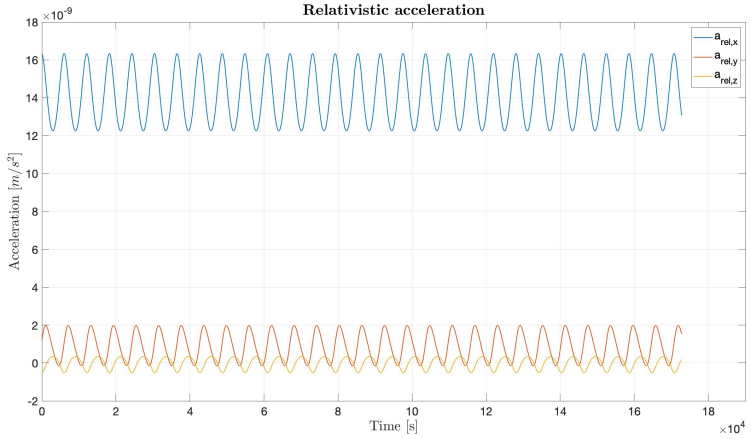

Figure 12: Relativistic acceleration in LVLH reference system

Figures 10, 11 and 12 show respectively the LVLH components of drag, SRP and relativistic accelerations.

The first important thing to underline is the order of magnitude of each contribution: 10^{-7} m/s^2 for drag, 10^{-8} m/s^2 for SRP and $10^{-9}/10^{-8}$ m/s^2 for relativistic. The drag-related acceleration is the highest and the one that influences the most the orbital dynamic.

Moreover, it's possible to see that the behaviour of all drag components presents some peaks and then some flat parts at about 0 m/s^2, confirming what has already been said. Indeed the peaks are in correspondence of the passes near the perigee (atmosphere's effect is not negligible), while the flat parts are in correspondence of the passes near the apogee (rarefied atmosphere and so very small resistance). The most important component is the y component, i.e. the along velocity component. This could be predicted both because the resistance of the atmosphere, like all fric-

tion forces, it's opposite to the velocity (indeed the y component is always negative) and because, as shown in Equation (4), $\mathbf{a}_{drag}$ vector is parallel to $\mathbf{v}_{rel}$.
The acceleration due to SRP, instead, presents two components that oscillate (x and y components), while the third (z component) is almost null. This is due to the fact that LVLH is a rotating frame, which changes following the satellite motion. While the z-axis is always parallel to itself, because the orbit is polar and the angular momentum is fixed, the x and y axes change with orbital periodicity. Furthermore, the solar rays are in x direction of ECI reference system and this leads the z component (in LVLH) of acceleration due to SRP to be null, because the z-axis is always perpendicular to solar rays and so photons don't reach z cross-section faces of the satellite. The other two components oscillates because they transform one into the other (with respect to ECI) during an orbit and solar rays hit sometimes the cross-section faces along velocity (when the satellite is near to the apsidal points) and sometimes the zenith cross-section face (when the satellite is crossing the equatorial plane).
All components of SRP-related acceleration have also some parts in which they're zero, because the satellite goes into eclipse behind the Earth, so that Sun isn't visible and solar rays don't reach the spacecraft. This can be seen better in Figures 13, 14 and 15, where the curves of each SRP component go to zero and then return to a different value.
Regarding the relativistic acceleration, Figure 12 shows how each component in LVLH is oscillating with a precise periodicity. The most important effect is along the zenith, because the higher term in Equation (6) is the Schwarzschild one and in particular the first part of that term, which is aligned to the position vector $\mathbf{r}$ (parallel to x-axis of LVLH). Indeed its contribution is at least one order of magnitude bigger than the other two components. Anyway acceleration due to relativity is the smaller effect between all the disturbing terms of equation of motion.
In the following figures the accelerations' components (of only three orbits) are divided and compared with the others in order to understand which effect is the dominant along each axis. Every figure presents drag (orange), solar radiation (yellow) and relativistic (light blue) acceleration relative to one axis and also the sum of the three contributions.

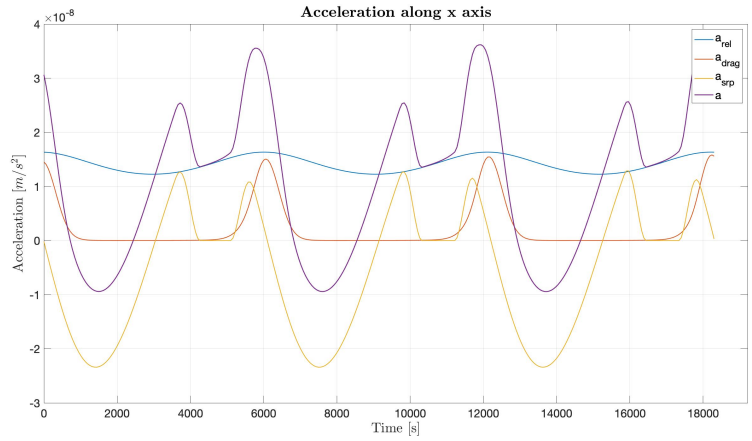

Figure 13: Drag, SRP and relativistic accelerations along x axis of LVLH

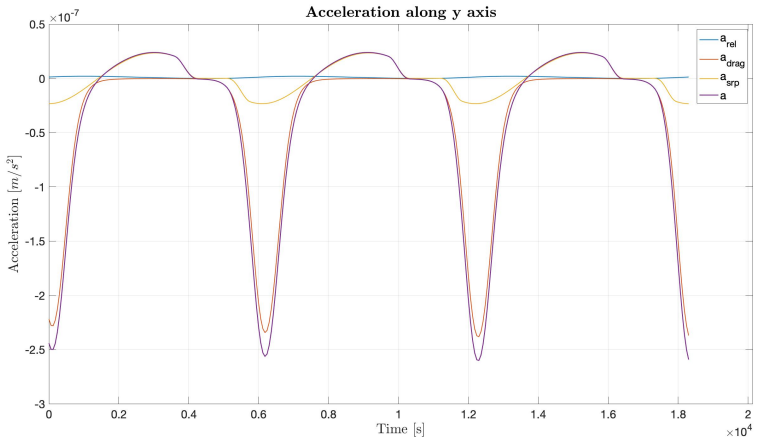

Figure 14: Drag, SRP and relativistic accelerations along y axis of LVLH

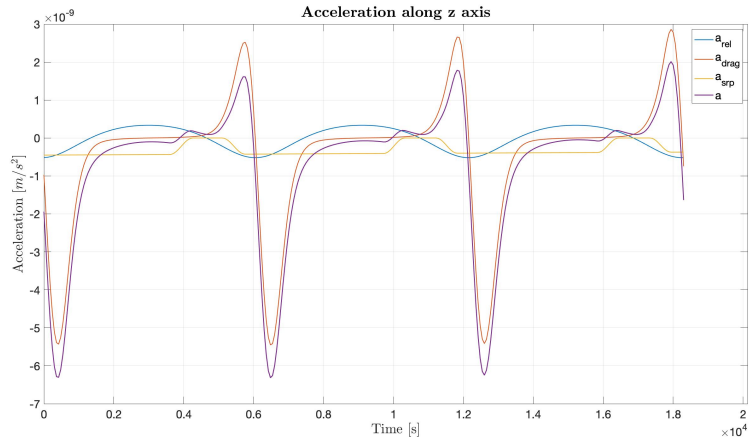

Figure 15: Drag, SRP and relativistic accelerations along z axis of LVLH

The accelerations along x-axis have almost the same intensity (order of magnitude of 10^{-8} m/s^2) so that the resultant is influenced in the same way by all effects.

As aforementioned, the drag contribution is characterized by some peaks in correspondence of the perigee, while SRP presents its highest value, in absolute terms, after the perigee, in particular, when the satellite crosses the equatorial plane. Indeed the ascending node is 90° after the perigee which is in the negative part of z-axis of ECI for assumption.
The relativistic correction, in the end, oscillates around a positive value of acceleration, bringing the total acceleration to increase.
Along y-axis, instead, the acceleration due to the resistance of the atmosphere is the dominant effect, because it is, at least, one order of magnitude higher than the others two. For this reason the y component's trend of the total acceleration follows almost completely the curve of drag component.
Moreover a_y is the higher component (order of magnitude of $10^{-7}\ m/s^2$) of the total resultant acceleration, indicating that the three contributions evaluated produces effects in particular on the along velocity direction.
The last component (on the perpendicular direction with respect to orbital plane), with an order of magnitude of $10^{-9}\ m/s^2$, is the smallest one. So the orbit is less perturbed along the z-axis of LVLH system.
Again, as for y-axis, the behaviour of the total z component is determined principally by drag.
Also Figures 16 and 17, which represent the resultant of drag, SRP and relativistic accelerations and its component, show that the most influential effect is along velocity (y-axis).
After the analysis of the single components it's possible to compare the total contributions of both non-gravitational and relativistic effects with each others.
Figure 18 shows what has already been stated: the acceleration due to drag is the higher in particular near the perigee, while near the apogee it decreases and the other effects become more important. Furthermore, while the SRP-related acceleration has a kind of step behaviour, the relativistic acceleration is oscillating around a mean value of some $10^{-8}\ m/s^2$.
Hence it's possible to assert that the orbit will be more influenced by the drag, if gravitational contributions are excluded, while the solar radiation pressure and the effects of relativity produce lower variations of the orbital parameters.

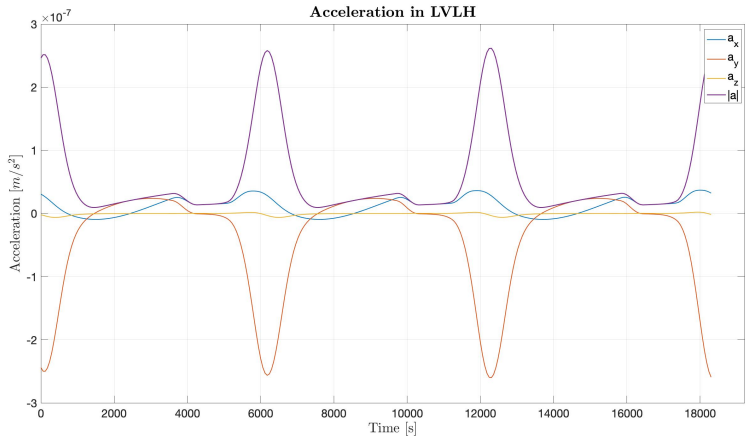

Figure 16: Acceleration due to drag, SRP and relativistic effects and its components in LVLH in three orbits

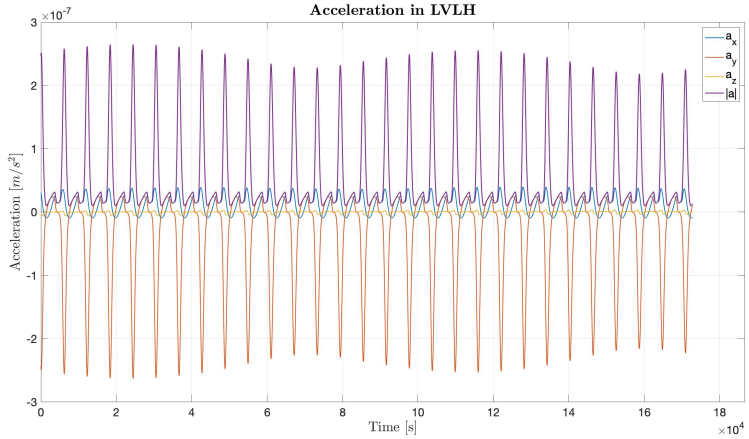

Figure 17: Acceleration due to drag, SRP and relativistic effects and its components in LVLH

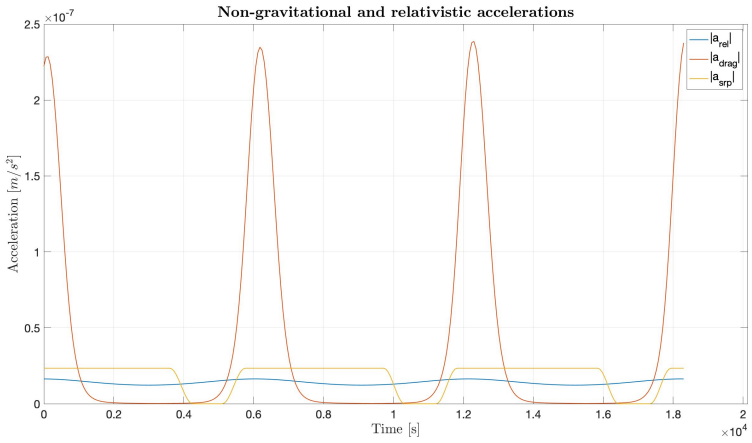

Figure 18: Non-gravitational and relativistic accelerations comparison

5.3.2 Spring equinox: orbital plane perpendicular to direction of solar rays

As aforementioned at the beginning of the previous paragraph, to change the operational situations, the initial state vector must be changed. In this case, where the orbital plane is perpendicular to the solar rays' direction at spring equinox, the initial state vector is:

$$\mathbf{y}_0 = \left\{0, \quad 0, \quad 0, \quad 7.837 \cdot 10^3, \quad -6.828 \cdot 10^6, \quad 0\right\}$$

Here the Sun, as above, is on the vernal point, so the orbital plane must lie on the y-z plane of ECI in order to be perpendicular to solar rays. The perigee is again assumed to be on the negative part of z-axis and therefore the initial velocity (always perpendicular to orbit because it's computed at an apsidal point) has only a y component, with the same value of the previous case because the shape of the orbit isn't changed but it's only rotated.
In Figures 19, 20 and 21 the results of the simulation are represented, with each contribution decomposed in its components of LVLH reference frame.
Drag and relativistic acceleration have a behaviour like that of the first case, so the considerations that can be done are the same.
However, the solar radiation pressure, instead, produces a different contribution. Figure 20 shows that there is in particular a component, that is almost constant, as principal effect. This is due to the orientation of the orbital plane and the position of the Sun on the ecliptic. Indeed this combination leads the cross-section face on z-axis (of LVLH) of the satellite to always see the Sun and to be always hit by the photons.

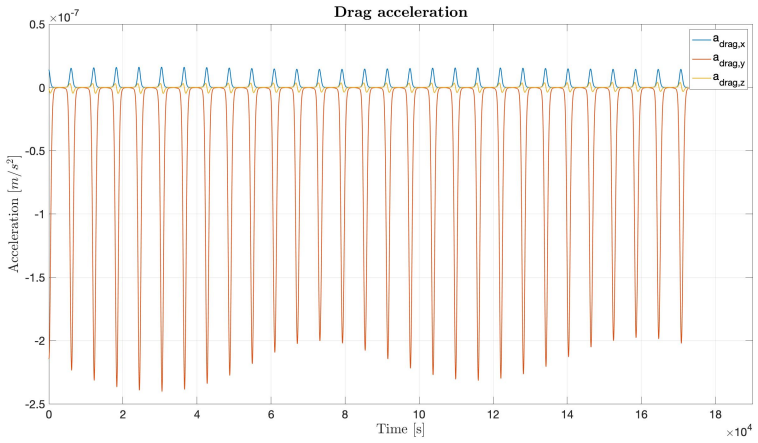

Figure 19: Drag-related acceleration in LVLH reference system

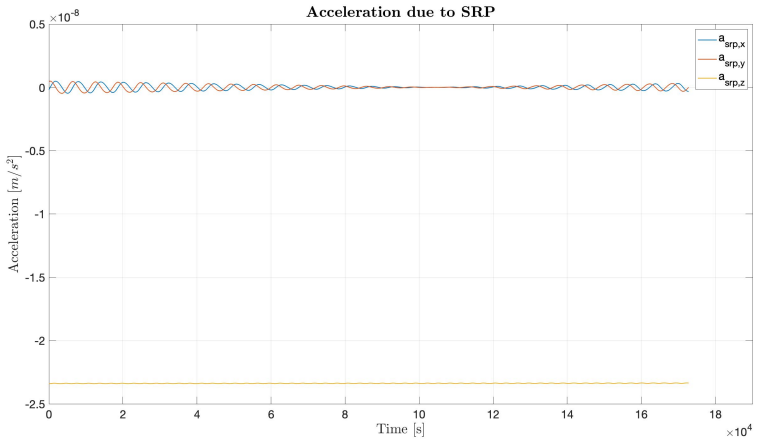

Figure 20: Acceleration due to SRP in LVLH reference system

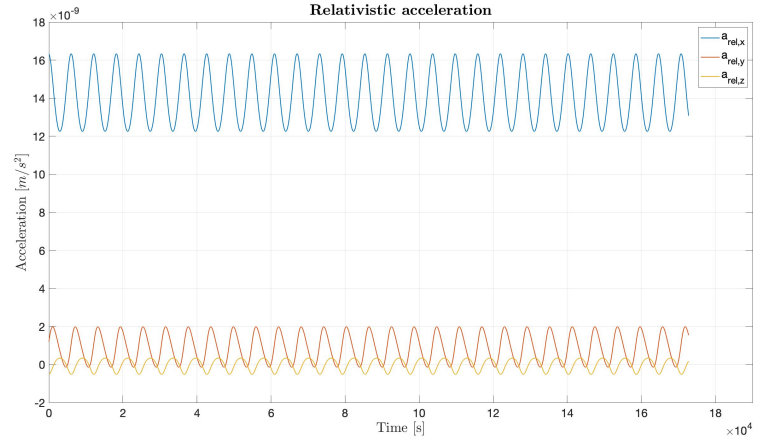

Figure 21: Relativistic acceleration in LVLH reference system

As the previous case, after the analysis of each contribution, the accelerations along each single axis of LVLH are discussed to understand how the resultant is influenced. Acceleration on the zenith direction (Figure 22) can be considered as the sum of drag and relativistic acceleration, which are also of the same intensity on this axis, especially near the perigee. The relativistic acceleration oscillates around a value of $\sim 1.4 \cdot 10^{-8}\ m/s^2$, shifting the resultant effect upward. SRP contribution is negligible with respect to the other two effects, because it is almost null.
In Figure 23 the along velocity accelerations are described. Even more than the first case, resultant and drag are similar, because, here, the effect of SRP is smaller than before and drag is again much greater than SRP and relativistic accelerations.
In the end, the total component of acceleration on z-axis is mostly influenced by the contribution of the solar radiation. Indeed, as shown in Figure 24, the relativistic component is the smallest, and the resultant is obtained considering the curve of

drag shifted downward by the SRP constant contribution.

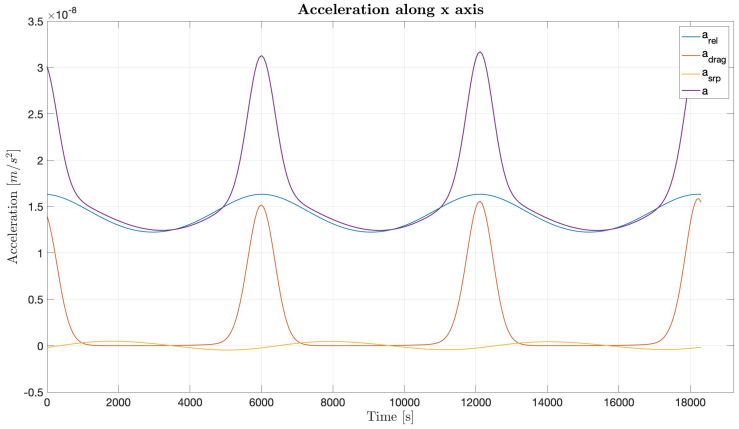

Figure 22: Drag, SRP and relativistic accelerations along x axis of LVLH

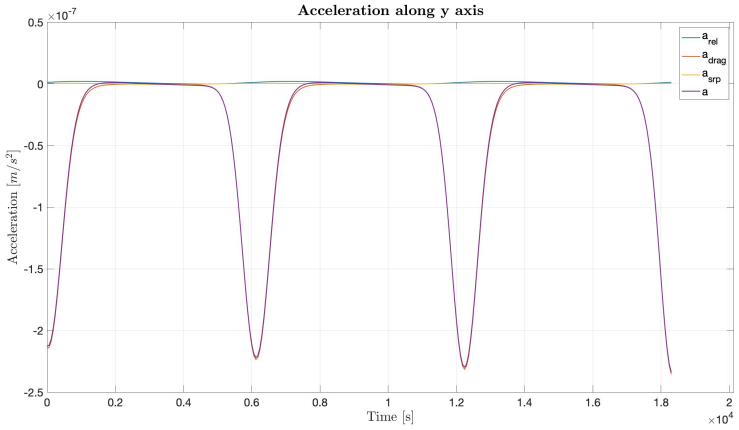

Figure 23: Drag, SRP and relativistic accelerations along y axis of LVLH

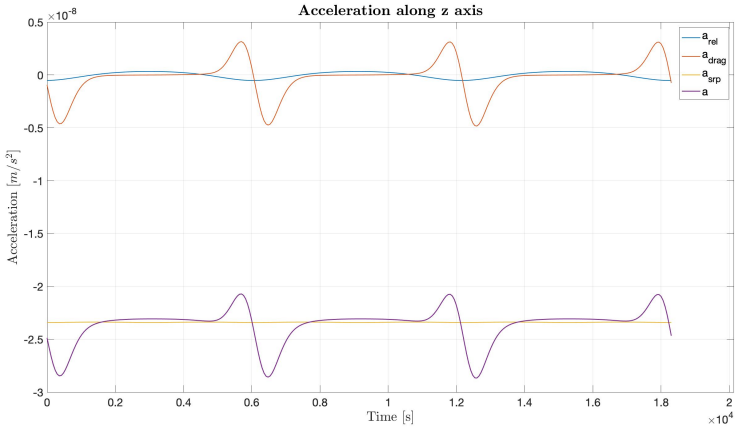

Figure 24: Drag, SRP and relativistic accelerations along z axis of LVLH

Also in these operational conditions the component with the higher intensity (10^{-7} m/s^2) is the y component, while the other two components are one order of magnitude lower (10^{-8} m/s^2).
This is shown in Figures 25 and 26. They represent the resultant acceleration and its components in LVLH, which are evaluated respectively on three orbits and on two days.
Moreover the drag is, as always, the most important contribution near the perigee while it's negligible near the apogee, where SRP and relativistic effects are higher, as represented in Figure 27, which compares drag, solar radiation pressure and relativistic effects.

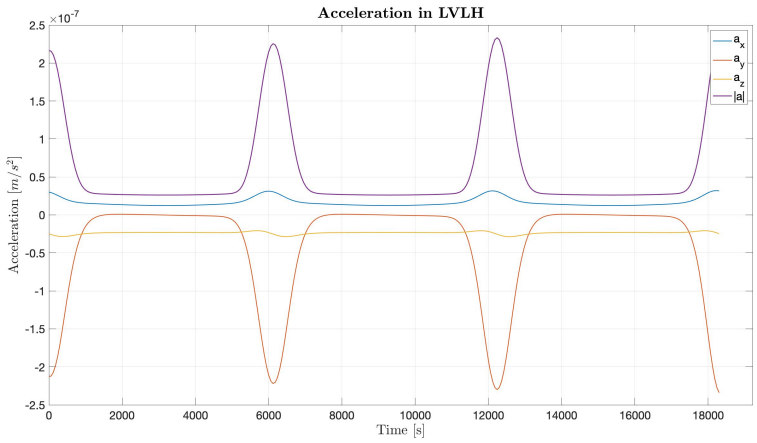

Figure 25: Acceleration due to drag, SRP and relativistic effects and its components in LVLH in three orbits

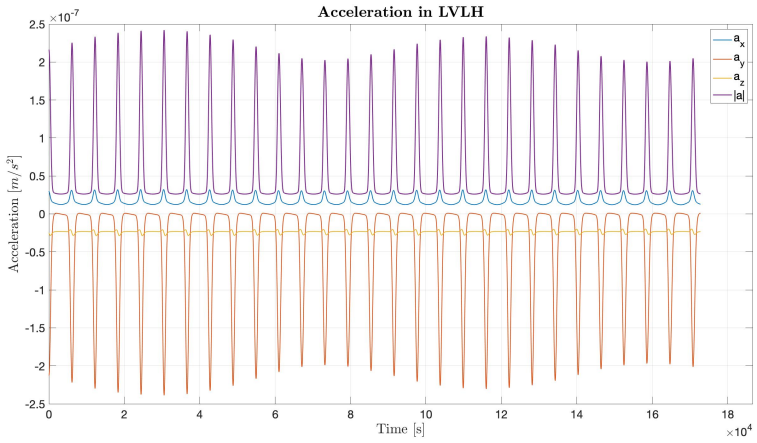

Figure 26: Acceleration due to drag, SRP and relativistic effects and its components in LVLH

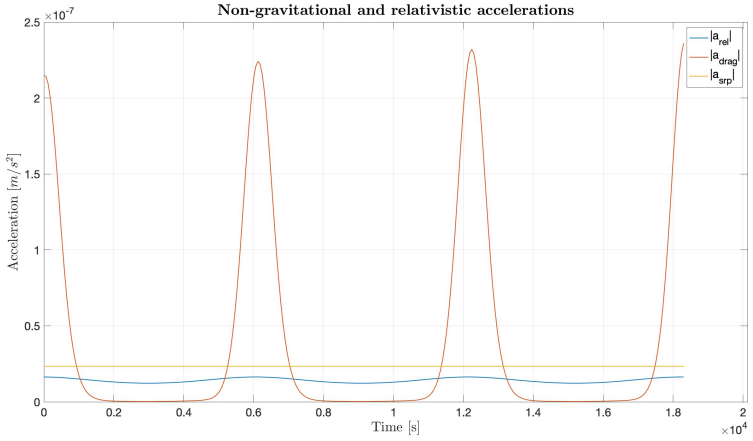

Figure 27: Non-gravitational and relativistic accelerations comparison

5.3.3 Summer solstice: orbital plane parallel to direction of solar rays

Differently from the previous, this case simulates the conditions that satellite undergoes during the summer solstice. Indeed the simulation's time, as for the next case, starts at 00:00:00 of 21 June 2023 and ends at 00:00:00 of 23 June 2023.
In that period the Sun is not anymore along the vernal direction, but it is rotated of 90° on the ecliptic, so it is along the y-axis of ECI. More precisely, the Sun is on a position on the y-z plane of ECI reference frame which forms an angle of about 23.5° with the positive direction of y-axis[10] due to the inclination of the ecliptic with respect to the equatorial plane. Anyway the direction from which the solar rays come is the y direction of ECI.
Consequently, assuming that the orbital plane has to be parallel to solar rays' direction, with the same argument as before, the initial state vector is:

$$\mathbf{y}_0 = \Big\{0, \quad 0, \quad 0, \quad 7.837 \cdot 10^3, \quad -6.828 \cdot 10^6, \quad 0\Big\}$$

It leads to an orbital plane that lies on y-z plane of ECI system, with the perigee again on the negative part of z-axis.
Drag (Figure 28) and relativistic accelerations (Figure 30) have the same behaviour of the previous cases, though the drag-related acceleration is a bit smaller (the highest peak has an amplitude of $\sim 1.3 \cdot 10^{-7}\ m/s^2$, while at the spring equinox it reaches $\sim 2.4 \cdot 10^{-7}\ m/s^2$), because the atmospheric density obtained by model is different between the two periods of the year, probably due to a different solar activity. The other parameters of Equation (4) don't change since they're geometrical parameters

[10] In Figure 8 it's possible to see the inclination of the Sun vector, which is not on the equatorial plane, but it's inclined.

related to the shape of the satellite, while the velocity is the same because the orbit doesn't change its form.
The relativistic effects, instead, are always similar with the other cases because they are dominated by Schwarzschild term, which is influenced in particular by position and velocity.
Acceleration due to SRP (Figure 29) is similar to the analogous configuration of orbital plane and Sun at spring equinox, with two oscillating components and one that is almost null.

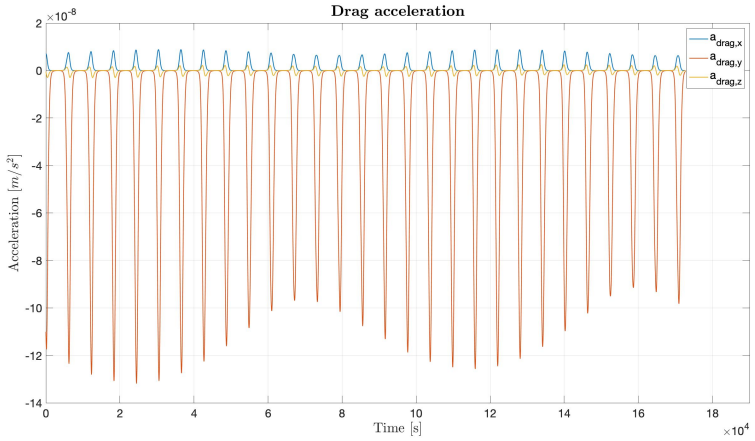

Figure 28: Drag-related acceleration in LVLH reference system

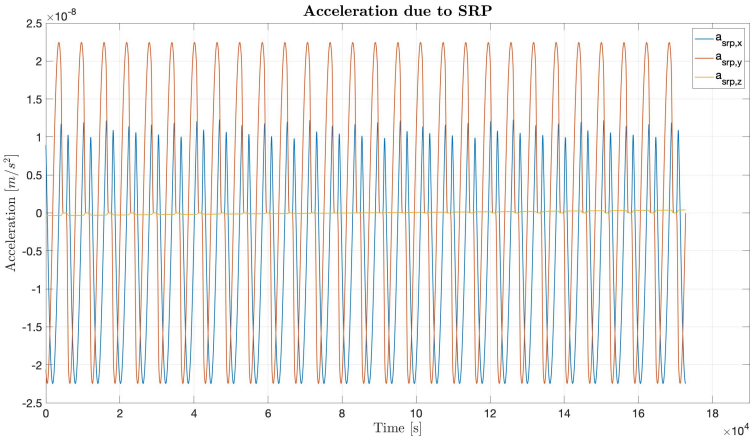

Figure 29: Acceleration due to SRP in LVLH reference system

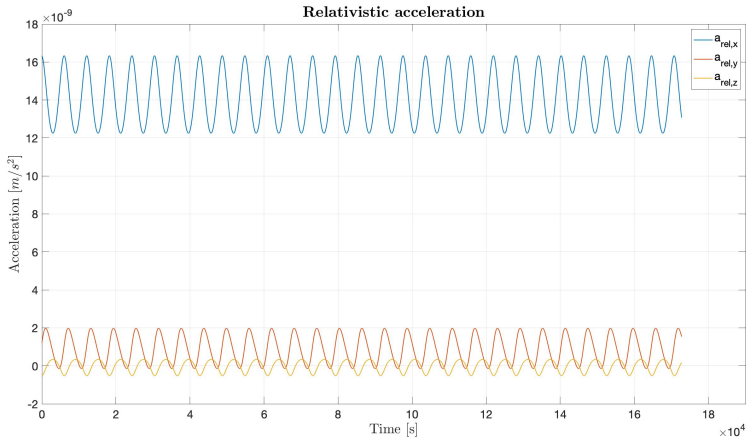

Figure 30: Relativistic acceleration in LVLH reference system

As above stated, this time, the contribution due to drag is smaller than before, and along the x-axis of LVLH system, in fact, the resultant acceleration is influenced more by SRP and relativistic effects, which are the higher in that direction.
Moreover Figure 31 shows that the peaks are shifted with respect to the analogous case at spring equinox[11] because of the angle that the Sun vector forms with the equatorial plane.
When the position vector of the satellite is aligned with the Sun vector the effect of solar radiation pressure is maximum and also the acceleration due to SRP along the zenith direction. Hence, while in the first case the peak is in correspondence of the ascending node, because the Sun was on the equatorial plane, here the peak is when the satellite is at 23.5° of elevation with respect to the Equator.
Along y-axis (Figure 32) and in the direction normal to the orbit (Figure 33), the accelerations' behaviour is similar to those at spring equinox with the orbital plane parallel to the direction of solar rays.
When the satellite is closer to the surface of the Earth, drag is dominant, and the resultant is quite completely determined by it. Instead, when the spacecraft is farther from the surface, SRP contribution is the the higher if the y-axis is considered (the y-component of acceleration due to general relativity is always at least two orders of magnitude smaller than the others contributions).
Along the normal direction to orbital plane, the acceleration is very low (order of $10^{-9}\ m/s^2$) and its most significant contribution is the drag, because the other two accelerations are of some $10^{-10}\ m/s^2$ and contribute in little part.

[11] See, for example, the second peak, which is quite before 8000 s in Figure 13 and almost at 8000 s in Figure 31.

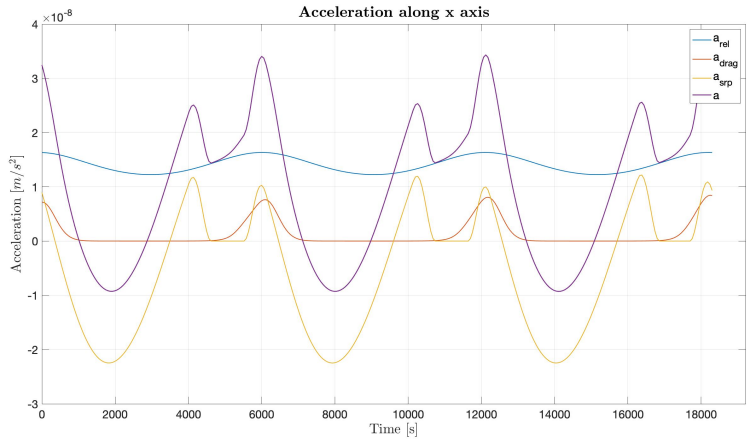

Figure 31: Drag, SRP and relativistic accelerations along x axis of LVLH

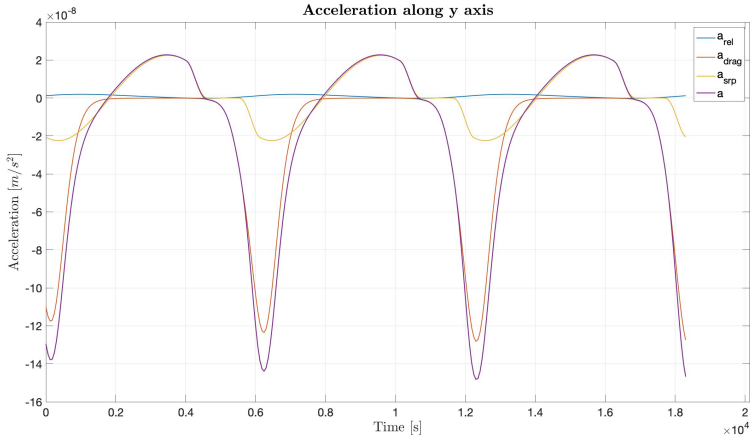

Figure 32: Drag, SRP and relativistic accelerations along y axis of LVLH

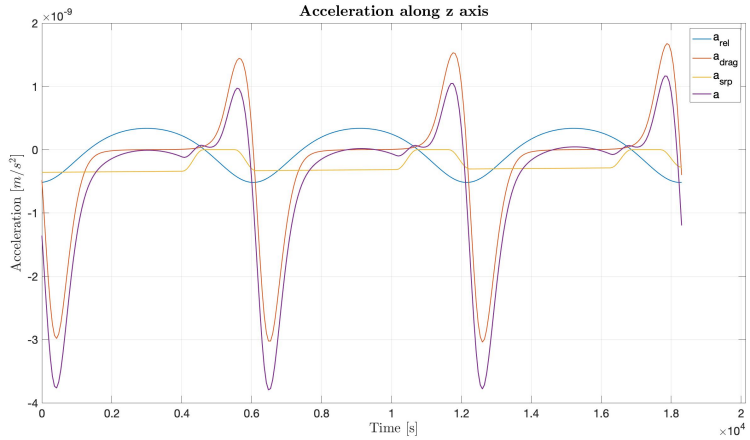

Figure 33: Drag, SRP and relativistic accelerations along z axis of LVLH

Figures above show also how the SRP has some falls to flat parts at 0 m/s^2 due to the eclipses periods to which satellite is subjected. Their duration is of about one

third of the orbital period.
Considering now the total components, it's possible to see (Figure 34 and 35) how, once again, the y component presents the higher peaks due to drag contribution, while SRP and relativistic effects are lower .
The z-component, in this situation, is almost null or very small with respect to the others, suggesting that orbit won't vary particularly in the direction parallel to the orbit's angular momentum.
In the end, Figure 36 compares the absolute values of both non-gravitational and relativistic accelerations, showing what has already emerged in the previous cases.

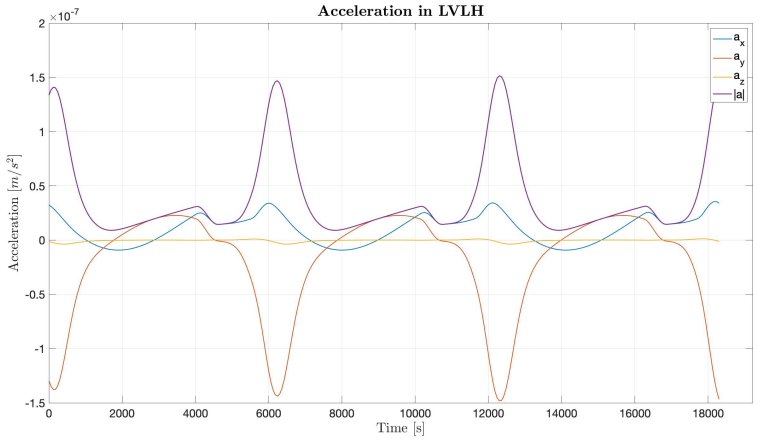

Figure 34: Acceleration due to drag, SRP and relativistic effects and its components in LVLH in three orbits

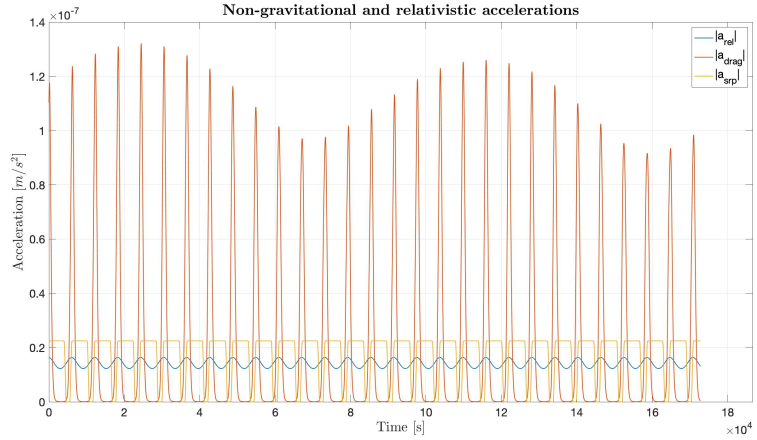

Figure 35: Acceleration due to drag, SRP and relativistic effects and its components in LVLH

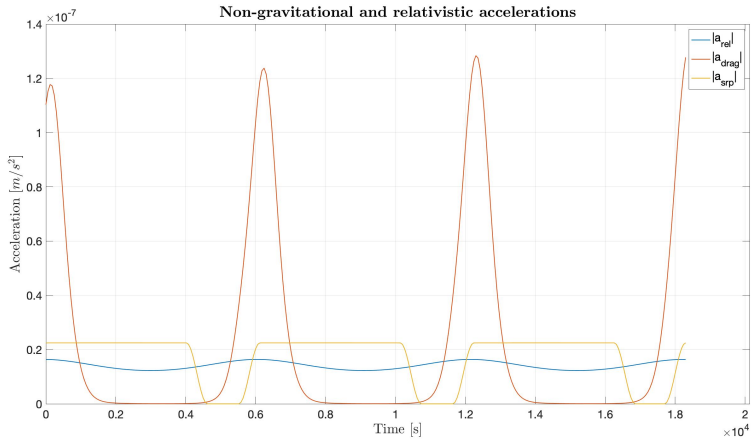

Figure 36: Non-gravitational and relativistic accelerations comparison

5.3.4 Summer solstice: orbital plane perpendicular to direction of solar rays

This is the last case analyzed in order to have an heterogeneous scenario of possible conditions to which the satellite can undergo, allowing to better evaluate the characteristics of the accelerometer.
The Sun is again lifted up of about 23.5° with respect to equatorial plane on the y-axis of ECI reference frame. So, if the orbital plane has to be perpendicular to the plane which contains the the solar rays (y-z plane), it has to lie on the x-z plane.
For these reasons, the initial state vector is like the first one (spring equinox with orbital plane orthogonal to solar rays' direction) because they described the same orbit

$$\mathbf{y}_0 = \left\{0, \quad 7.837 \cdot 10^3, \quad 0, \quad 0, \quad -6.828 \cdot 10^6, \quad 0\right\}$$

Also with this operational conditions, drag acceleration (Figure 37) has peaks with smaller amplitude than those at spring equinox, confirming that atmospheric density at summer solstice is lower, probably due to a different solar activity. Moreover the most important component of drag is, as always, the component along velocity, in the opposite direction of motion (indeed the component is negative).
Relativistic effects, which are shown in Figure 39, are of low intensity and oscillate like in the other cases. The higher component of this acceleration is the component along x-axis (zenith) due to the fact that Schwarzschild term is the most important and it's parallel with the position vector (hence zenith too), as above stated.
The SRP contribution (Figure 38), then, is a bit different from the analogous case at spring equinox. The z component (of LVLH) is almost constant, as could have been predicted, but has some falls. This behaviour is linked to eclipses. Indeed the

satellite goes into eclipse (for a short time) when it passes near the perigee, because the shadow of Earth is tilted and not parallel to equatorial plane due to the inclination of the ecliptic with respect to Equator and the perigee is at low altitude.
The other two components of SRP acceleration oscillate with larger amplitudes than those studied at spring equinox with the orbital plane perpendicular to the direction of solar rays, again because of the inclination of solar rays with respect to the x-z plane of ECI (where the orbit lies). Indeed, also parts of faces along zenith and velocity see the Sun and are hit by the photons, leading to an acceleration in those directions too.

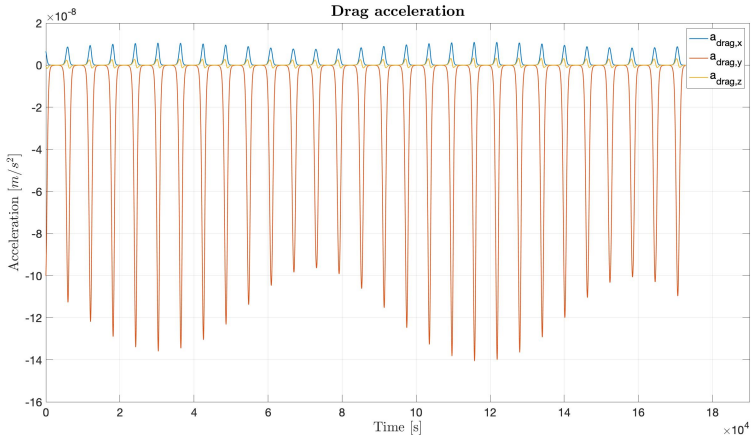

Figure 37: Drag-related acceleration in LVLH reference system

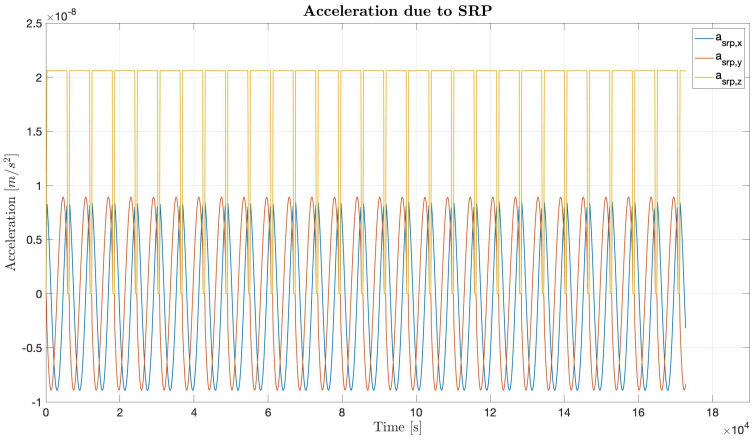

Figure 38: Acceleration due to SRP in LVLH reference system

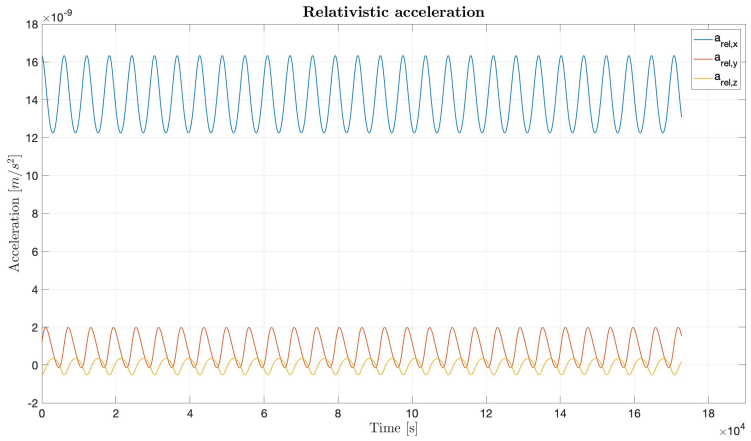

Figure 39: Relativistic acceleration in LVLH reference system

Considering all components of each acceleration's contribution, the first thing that emerges is that, along the x-axis of LVLH (Figure 40) all effects have similar intensities and contribute equally to the resultant.
Furthermore, as aforementioned, when the satellite is near the perigee the drag (orange line in Figure) has some peaks and SRP (yellow line) has falls due to eclipses. The solar radiation is instead significant near the apogee (between two consecutive peaks of drag), because the Sun vector's inclination allows the zenith face, which is aligned with z-axis of ECI in that point, to be partially hit by solar rays.
Acceleration component due to relativistic effect oscillates around a positive mean value, shifting the total contribution upward.
Figure 41 shows the acceleration's contributions and their resultant along y-axis of LVLH. As the previous cases, drag is the higher contribution and the resultant follows its behaviour, except near the apogee, where the SRP is more important. Anyway the peaks of acceleration due to drag are at least one order of magnitude higher than the order effects, especially those of relativity.
Then, the last component, i.e. the component along the normal direction to orbital plane (see Figure 42), is dominated by the effect of solar radiation pressure. Only near the perigee, when the satellite goes into eclipse, its effect decreases and also the total acceleration (purple line) along this axis. However, the eclipses don't last for a long time, so the total acceleration along z-axis of LVLH can be considered almost always equal or close to the peak value of z component of SRP acceleration. Here, the relativistic acceleration is very small because it is in the order of 10^{-10} m/s^2, and so its contribution is not important in the perturbation of orbit with respect to the others.

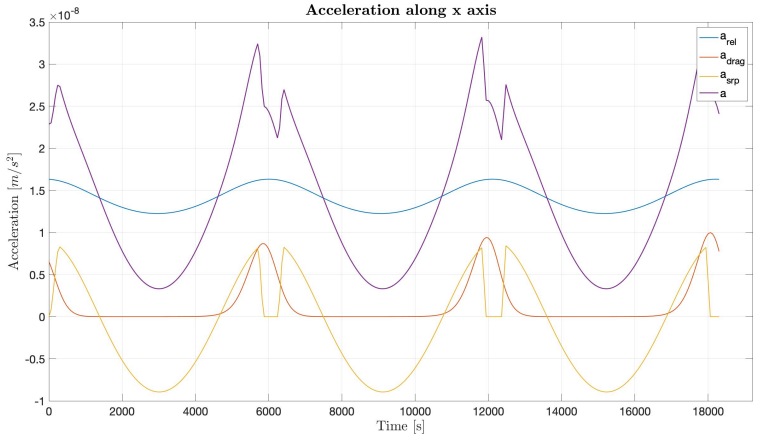

Figure 40: Drag, SRP and relativistic accelerations along x axis of LVLH

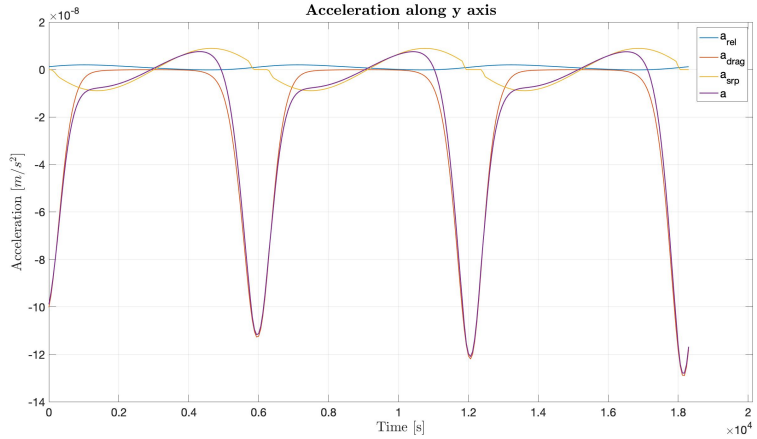

Figure 41: Drag, SRP and relativistic accelerations along y axis of LVLH

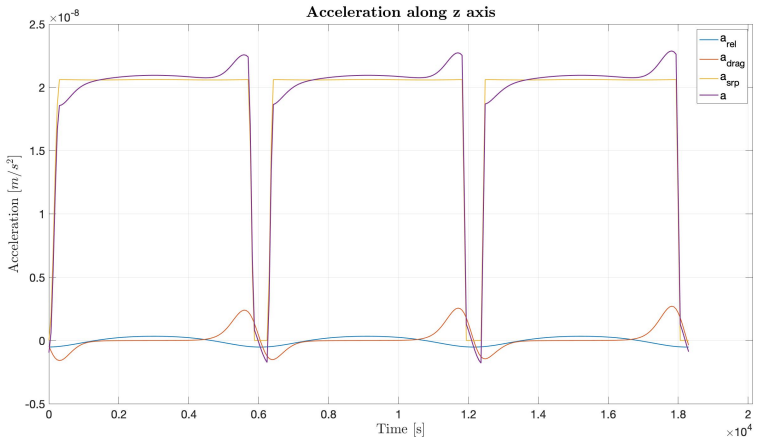

Figure 42: Drag, SRP and relativistic accelerations along z axis of LVLH

Finally, observing Figures 43 (representation of total acceleration and its components), 44 and 45 (in which the absolute values of the single contributions along all

simulation's time and then only for three orbits are shown), it is possible to conclude that:

- the drag is once again the contribution with the higher effects (order of $1 \cdot 10^{-7}$ m/s^2);
- the solar radiation pressure produces an acceleration almost constant in particular along the z-axis of LVLH reference system;
- the effects due to relativity are oscillating and, always in the order of 10^{-8} m/s^2.

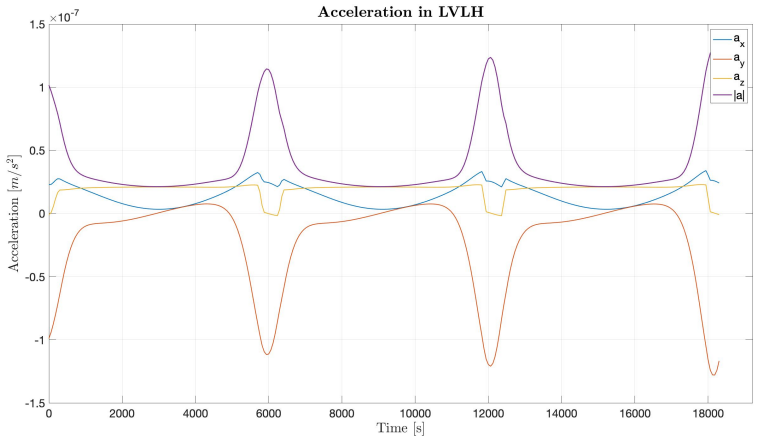

Figure 43: Acceleration due to drag, SRP and relativistic effects and its components in LVLH in three orbits

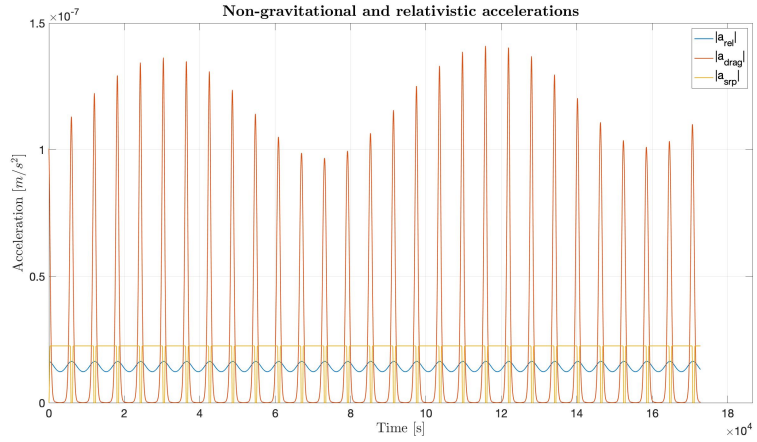

Figure 44: Acceleration due to drag, SRP and relativistic effects and its components in LVLH

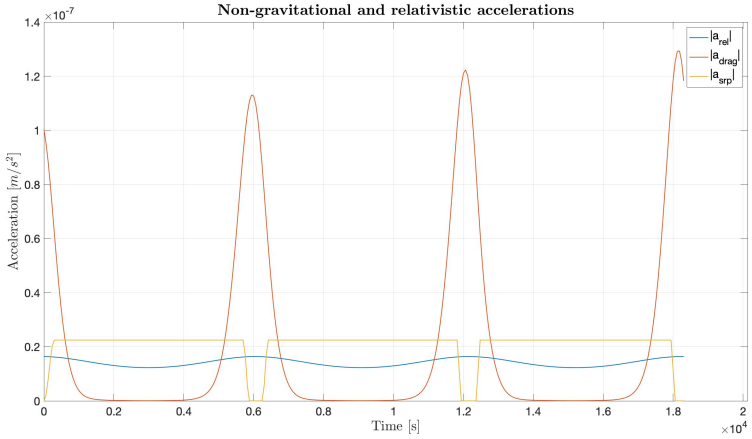

Figure 45: Non-gravitational and relativistic accelerations comparison

The simulation of the satellite scenario at summer solstice with orbital plane perpendicular to solar rays' direction ends the first part of the work where the accelerations to which the satellite is subjected have been computed.
In general, the results of every case are coherent with the others. The differences are due to the different conditions of evaluation, as initially wanted, in order to have a complete idea of all possible forces.
Results obtained confirm the initial idea to consider the non-gravitational forces in different parts of the orbit (apsidal points), through continuous measurements, in order to separate their effects post-flight.
Now, starting from these data, the spectral analysis of the non-gravitational accelerations is carried on in order to compute also their band of frequency.
The relativistic accelerations have been estimated, instead, to understand only how much they influence the total acceleration with respect to non-gravitational effects, i.e. if they are bigger or smaller than drag or SRP and on which axes. Indeed the effects of general relativity aren't measured by the accelerometer, so they have to be computed in another way (through a post processing procedure with tracking data, which is discussed in Chapter 6).

5.4 Results of spectral analysis

As for the accelerations of the dynamical simulations, also the spectral analysis presents the four cases of operational conditions. The accelerations previously computed are evaluated with the Fourier analysis as said in paragraph 4.4.
Remembering that the Fourier analysis consists in the representation of a signal as the sum of some sinusoidal terms with different amplitude and frequency, this procedure is done for both the absolute value of each non-gravitational acceleration (drag-related and due to SRP) and all their components, in order to completely analyzed them.
Spectral analysis concerns only accelerations due to drag and SRP because they're the contributions measured by the accelerometer. Their frequency spectrum will then be considered in order to evaluate the bandwidth of the instrument.

5.4.1 Spring equinox: orbital plane parallel to direction of solar rays

Considering the accelerations of the first situation, the power spectral density of the drag contribution is shown in Figures 46 and 47. Both for the absolute value of the acceleration and for its components, it emerges that several terms with increasing frequency and decreasing amplitude can be considered to model this effect. Indeed, observing the Figures relative to drag of the previous paragraphs, this effect hasn't an oscillation with constant amplitude, bringing to have a sum of different sinusoidal terms as approximation of it.
Furthermore, the highest peak, which represents the most important term in the series, is in correspondence of the orbital frequency (indicated by the dashed vertical line), which is about $1.6 \cdot 10^{-4}\ Hz$, i.e. the inverse of the orbital period. This suggests that the effects of the drag, in first approximation, repeat once every orbit.
However, also the second peak has a PSD value similar to the first one, so it is important too. It has a frequency which is double of the orbital frequency due to the fact that drag is proportional to the velocity squared. From Equation (4), it can be written that $\mathbf{a}_{drag} \propto v\mathbf{v}_{rel} \propto v^2\hat{\mathbf{v}}_{rel}$ and so $a_{drag} \propto v^2$. As the value of the velocity varies periodically (period equal to the orbital one) it can be expressed as a sine, and so if $v \propto sin(f(t))$, the square of the velocity $v^2 \propto sin^2(f(t)) = \frac{1}{2}[1 - cos(2f(t))]$ and more generally $v^2 \propto cos(2f(t))$, indicating precisely the double frequency.
Anyway, all components of drag have also the same PSD behaviour, because the total effect of drag itself and consequently of its components, increases near the perigee and then decreases near the apogee. This leads the components to have similar power spectrum.

For lower frequencies the curves tends to a constant value, suggesting that there is a component with small frequency, i.e. almost constant in time. Its amplitude is, anyway, smaller than that of the highest term.

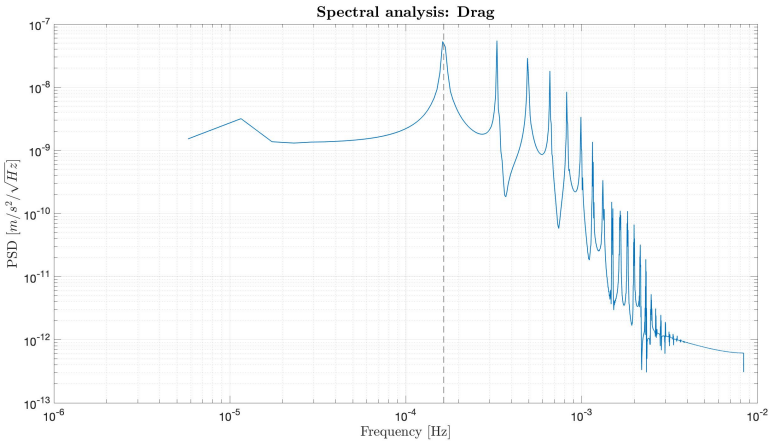

Figure 46: Power spectral density of drag acceleration

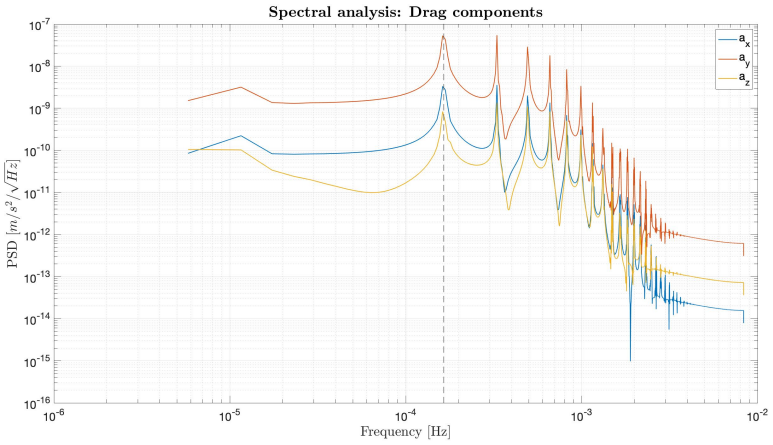

Figure 47: Power spectral density of drag acceleration's components

Concerning the accelerations due to SRP (Figure 48), the fundamental sinusoid (the one with the highest PSD) is again at orbital frequency and there's another significant term with frequency which is double than the first. Then there are other terms at higher frequencies with decreasing amplitude. The reason of these peaks, in this case, is that the solar radiation pressure doesn't act continuously on the satellite due to the eclipses, so there is a step like behaviour and the power spectrum of a step is an infinite series of terms with increasing frequency and decreasing amplitude.
Observing Figure 49, each component has the peaks in correspondence of the same frequencies, and especially x and y components are similar also in amplitude. They

differs in particular in the constant value (low frequency).
The behaviour of z component is quite peculiar, indeed the PSD tends to increase towards the lower frequencies with values higher than the peak in correspondence of the orbital frequencies. This is due to the fact that the z component is almost constant, as shown in Figure 11.

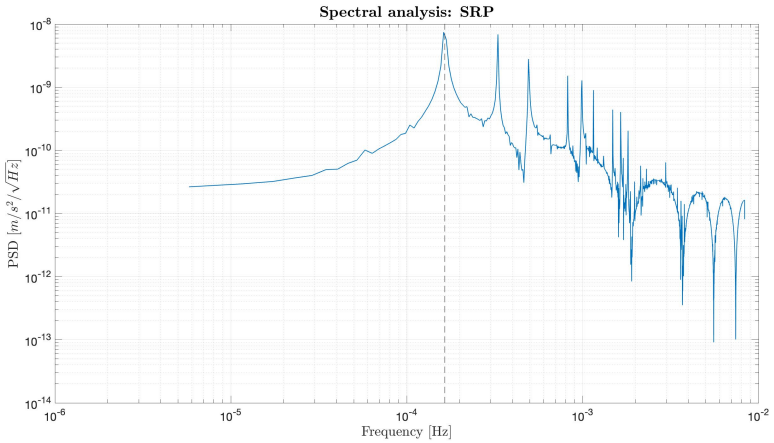

Figure 48: Power spectral density of SRP acceleration

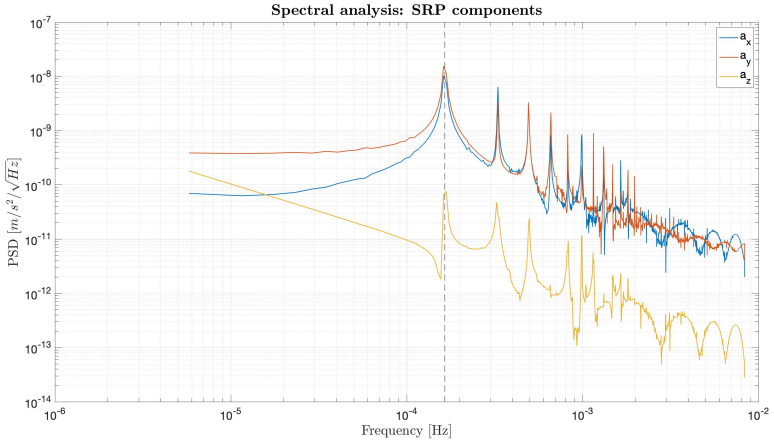

Figure 49: Power spectral density of SRP acceleration's components

In conclusion, for this case, all non-gravitational contributions present the higher term of the relative power spectrum in correspondence of the orbital frequency and have smaller terms with higher frequencies.

5.4.2 Spring equinox: orbital plane perpendicular to direction of solar rays

When the orbital plane is perpendicular to the direction of solar rays, the behaviour of the drag is not so different from the previous case. The most significant peak is at

orbital frequency and then there are terms with decreasing amplitude and increasing frequency. Also in this case, a small constant contribution is present both for the resultant and for each component. Figures 50 and 51 show what has just been stated.

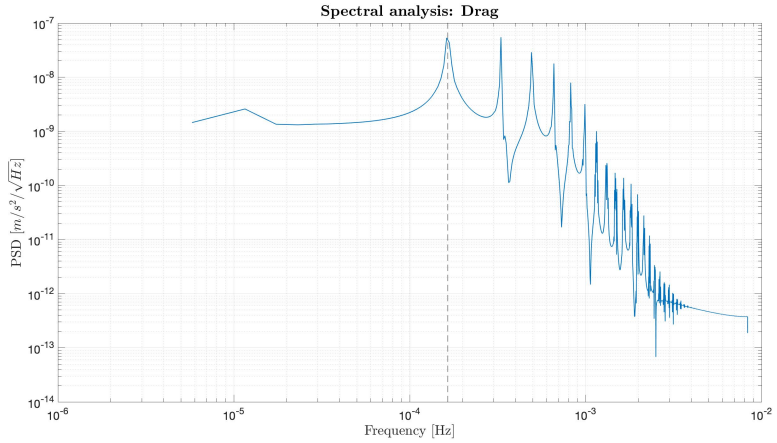

Figure 50: Power spectral density of drag acceleration

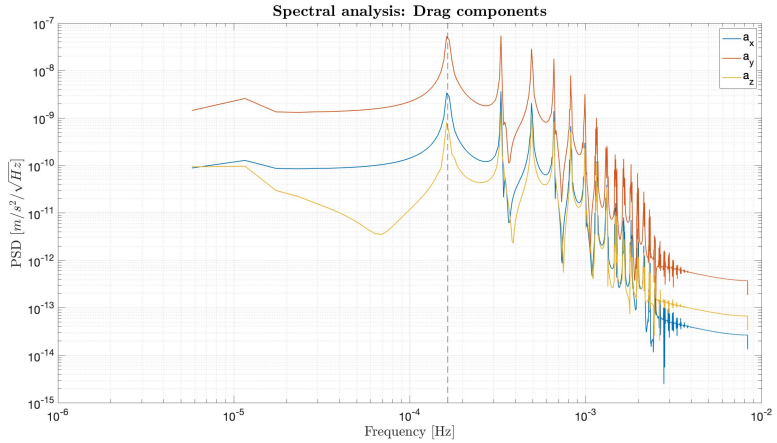

Figure 51: Power spectral density of drag acceleration's components

Differently, the spectral analysis of SRP is more interesting. Indeed, as presented in Figures 52 and 53, the overall trend is increasing toward lower frequencies, indicating that the most important term is a constant term. Anyway the intensity of PSD is lower than the value found with the simulations relative to SRP acceleration, because the spectral analysis removes from the signal analyzed the constant mean value and then studies the remaining oscillating signal, so the contribution of a constant value is not presented in the PSD.
The power spectrum of the resultant acceleration is determined especially by the z

component (the most significant, see Figure 20), which is almost constant (about $-2,4 \cdot 10^{-8}\ m/s^2$) but presents also oscillations with very small amplitude. Indeed their PSD is of the order of $10^{-11}\ m/s^2/\sqrt{Hz}$ and can be considered negligible with respect to the constant term, but, as aforementioned, this doesn't compare in the PSD plot.

Furthermore, x and y components have higher peaks at orbital frequency than that of z component, because they are oscillating components (see again Figure 20), and so they can be described by a single sinusoidal term better than the other component which is almost constant. This is the reason why x and y components have higher peaks in the PSD in Figure 53, though they're lower in absolute value.

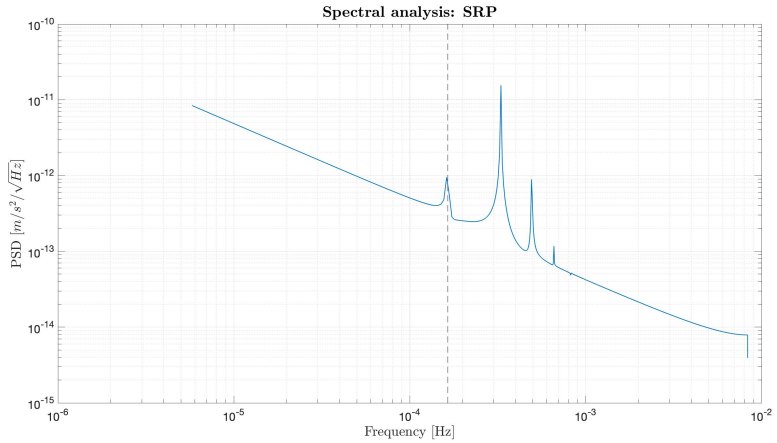

Figure 52: Power spectral density of drag acceleration

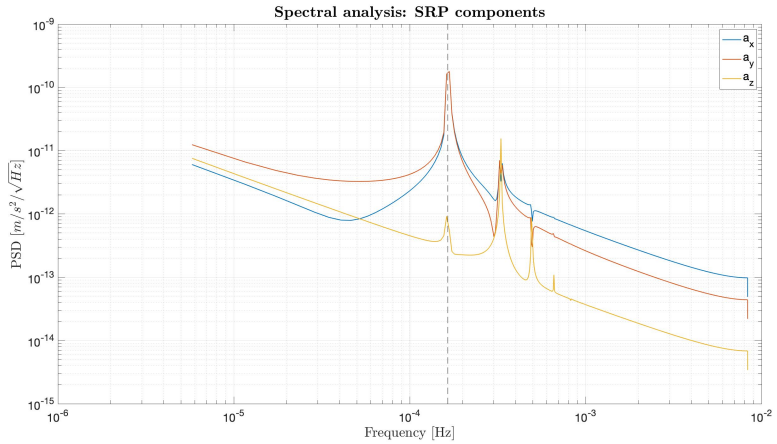

Figure 53: Power spectral density of drag acceleration's components

5.4.3 Summer solstice: orbital plane parallel to direction of solar rays

The spectral analysis of the accelerations obtained from the simulation at summer solstice with the orbital plane parallel to the direction of solar rays gives similar results to those of the previous cases.
Drag has once again the trend seen before, with the difference that, as mentioned in the previous paragraphs, the total effect is lower than the relative one at spring equinox. So the peaks visible in Figures 54 and 55 are at lower values of PSD than the analogues of Figures 46 and 47.

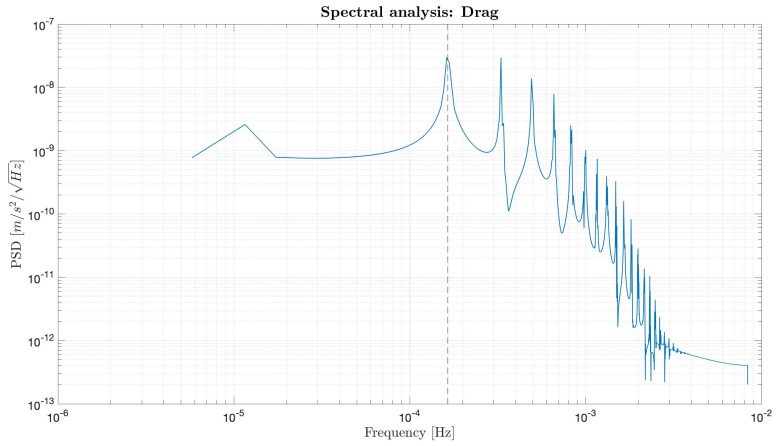

Figure 54: Power spectral density of drag acceleration

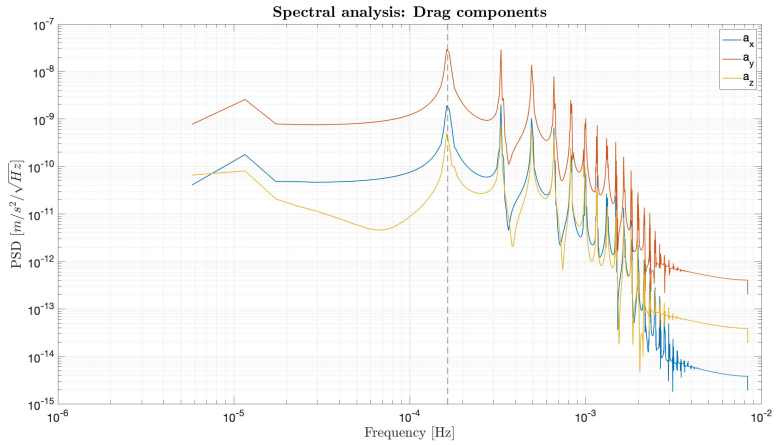

Figure 55: Power spectral density of drag acceleration's components

Also for the accelerations due to SRP there are no differences with the previous case where the orbital plane was parallel to solar rays' direction.
The fundamental frequency is always the orbital frequency and then there are other

terms that model the studied acceleration with higher frequency and lower amplitude, indicating, as above stated, that they're less significant in the approximation. The following Figures (56, 57) show the analysis of accelerations due to SRP.

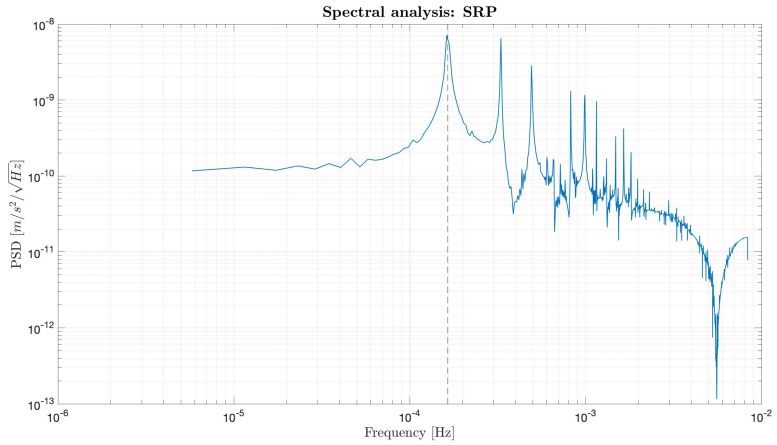

Figure 56: Power spectral density of SRP acceleration

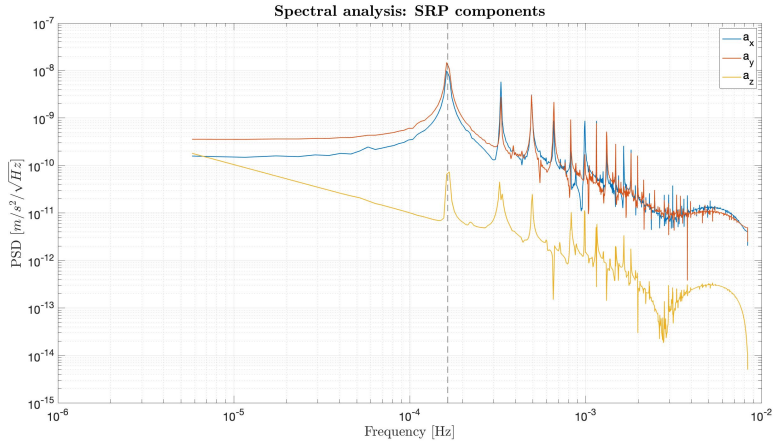

Figure 57: Power spectral density of SRP acceleration's components

5.4.4 Summer solstice: orbital plane perpendicular to direction of solar rays

This case is the last one but it is similar to the cases already seen. Indeed drag has the same behaviour of all situations, and, as the previous one, the amplitude of the peaks is lower than those of spring equinox due to the decreasing of the drag acceleration caused by a reduction of the atmospheric density computed with the NRLMSISE-00 model.

Figure 58 and 59 present the PSD of the drag acceleration and suggest that this effect is principally modulated with a periodicity of one orbital period and then

with terms with shorter period. The component have similar trend with each other and also with the total acceleration. Moreover their PSD confirm that the major contribution is along y component, i.e. the drag is more significant on the along velocity direction.

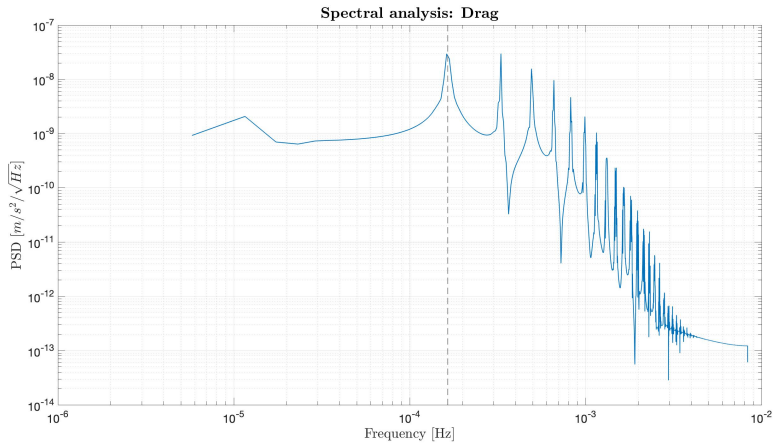

Figure 58: Power spectral density of drag acceleration

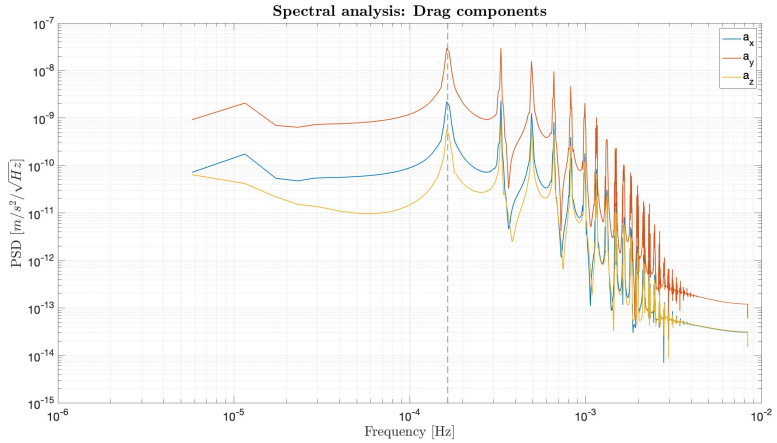

Figure 59: Power spectral density of drag acceleration's components

Solar radiation pressure, in this situation, presents characteristics similar, but not equal, to the other cases. Indeed the power spectrum is more oscillating than the others and especially the component along the normal direction to orbital plane present a lot of peaks (Figure 61). The reason is that the length of the eclipses is very small, so the z component is like a step function because it passes rapidly from a value of acceleration of $\sim 2 \cdot 10^{-8}\ m/s^2$ to zero and vice-versa. As aforementioned, the step function has a spectrum with infinite terms.
Furthermore the absolute value of SRP acceleration (Figure 60) shows more peaks

with similar PSD, suggesting that the variations of this effect are also faster, and the terms at higher frequency have an amplitude that decreases more slowly than that of the other analyzed situations.

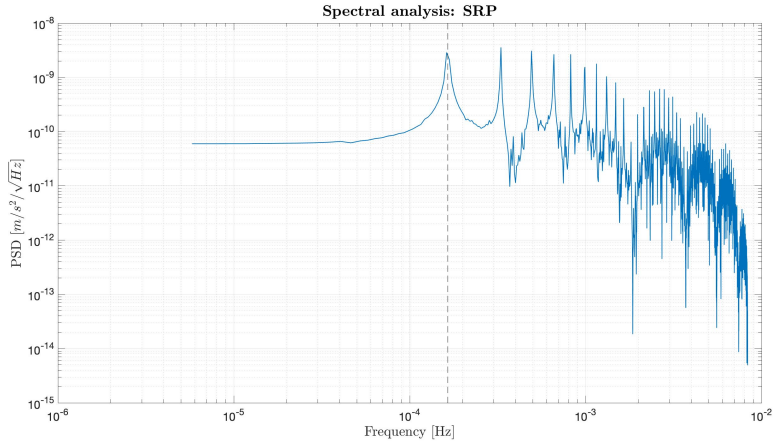

Figure 60: Power spectral density of SRP acceleration

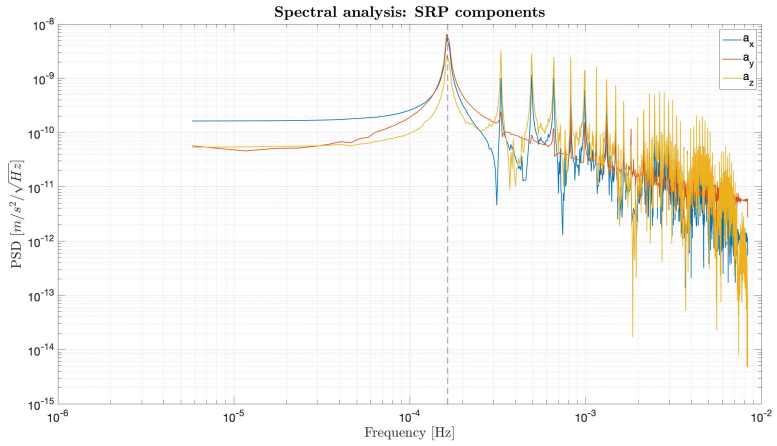

Figure 61: Power spectral density of SRP acceleration's components

With this case also the spectral analysis is completed, so that it's possible to think about the bandwidth of the accelerations and consequently of the accelerometer.
Generally, considering all cases that has been studied, it's possible to highlight that both drag and SRP accelerations have a common fundamental frequency which corresponds to the orbital frequency (about $1.6 \cdot 10^{-4}\ Hz$). Then there are some contributions, such as SRP, that present constant values, indicated by terms of low frequency on the PSD.
In the end, also terms with frequency higher than the orbital one have to be consid-

ered because some of them have not negligible power, and the accelerometer must be able to measure them too.

6 POD: Precise Orbit Determination

The orbital determination is a problem that started with studies about the motion of planets, in order to determine their paths around the Sun. Nowadays the determination of orbits is needed also for satellites, because it allows not only to know their positions and predict them through mathematical model, but this measurement is used for scientific purposes, like geodesy, too.
Different techniques can be used to track satellite, but the most important is the Satellite Laser Ranging (SLR)[4]. It consists in the measurement of the range (i.e. the distance) between several ground stations and the satellite, through the evaluation of the time of flight of laser beams, which leave the station, hit the satellite and then are reflected by special reflectors and return to the station.
SLR is the most accurate technique currently available which allows to determine the orbital position of satellites in a geocentric system. Indeed it's possible to reach an accuracy of the order of some centimeters in the estimation of spacecraft's position.

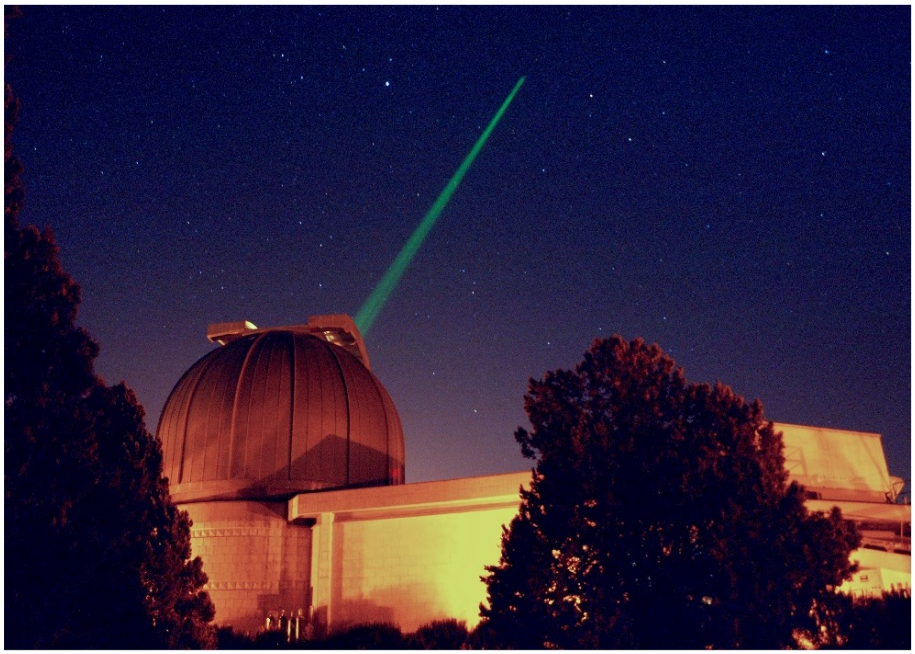

Figure 62: Example of SLR. Credit: ASI-CGS

As above stated, METRIC satellite will foresee retroreflectors on its external surface allowing the tracking from ground and the precise orbit determination.
In this thesis Matera laser ranging observatory is considered as the ground station that has to evaluate the position of METRIC spacecraft. Through an Event Locator [3] of GMAT the possibility that this station can see and track the satellite is

assessed. Assuming a cut off angle of 10°, so that the spacecraft can't be tracked if it has an elevation with respect to the local horizon of the ground station below that angle, the chosen station can usually track the satellite (about thirty passes every ten days).
After having verify that it's possible to perform POD with Matera laser ranging observatory, some simulations are done in order to compute what can be evaluated collecting lots of data in time, especially the drifts of the Right Ascension of Ascending Node (RAAN) and of the Argument Of Perigee (AOP).
The simulations use the dynamical model already presented but last seven days instead of two, because the variations of RAAN and AOP due to drag, SRP and relativity are quite small (order of $arcsec/year$) and so they can be observed only in long periods.
All simulations are at spring equinox with the orbital plane perpendicular to the direction of solar rays because, in this way, the contribution of SRP is constant in time (worst case). The differences between the simulations are the acting forces considered in the equation of motion:

1. all forces (gravitational, drag, SRP) and also relativistic corrections are considered, as simulations of Chapter 5;
2. non-gravitational forces (whose effects are limited to a threshold of $10^{-8}\ m/s^2$), spherical term of gravity and relativistic effects;
3. non-gravitational forces (whose effects are limited to a threshold of $10^{-9}\ m/s^2$), spherical term of gravity and relativistic effects;
4. non-gravitational forces (whose effects are limited to a threshold of $10^{-10}\ m/s^2$), spherical term of gravity and relativistic effects;
5. non-gravitational forces (whose effects are limited to a threshold of $10^{-11}\ m/s^2$), spherical term of gravity and relativistic effects;
6. only spherical term of gravity and relativistic corrections.

The first case considers and simulates the real situation in which satellite undergoes. Then, situations from 2 to 5 are thought in order to evaluate what changes varying the accuracy of the accelerometer. It, as aforementioned, measures only the non-gravitational accelerations. Once known, their effects can be removed from the data of tracking, leaving only the contributions of relativity and gravity. Also the effects of non spherical terms of gravity can be removed too using the known models, so that, at the end, the effects of general relativity can be evaluated. Increasing the accuracy, the measured effects of drag and SRP should be more precise and closer to the "real" ones, and so, in post-processing, the relativity can be better estimated.

However, if drag and SRP contribute with accelerations lower than acceleromter's accuracy, their effects can't be evaluated and act as a noise for the relativistic ones. The simulations aims to reproduce the results of the post-processing procedure, so the non-gravitational accelerations are limited to values lower than the accuracy of the instrument as if the higher values have already been removed.
The last case has to give the ideal drifts due to only relativistic terms and should represent the target to which the other cases must approach.
Furthermore, before the mentioned situations, also another case is studied, which is based on the equation of motion with only the spherical term of gravity. It can be consider as a benchmark that allows to find possible errors (due to integration or machine errors). Indeed the gravity due to a perfect spherical body doesn't influence the orbital parameters which must remain fixed. So, if the drifts founded with this simulation are different from zero as they should be, they are removed from the other cases in order to cancel the undesired errors.
After each simulation the position vectors are transformed from Cartesian coordinates to Keplerian coordinates, obtaining especially RAAN and AOP at very step of integration.
Assuming the case with only the effects of the spherical term of gravity and the relativistic effects as reference case, the absolute errors on both parameters are computed. They represent the differences, in *arcsec*, between the reference case and the others due to non-gravitational accelerations that accelerometer can't measure. Figures 63 and 64 show the absolute errors of RAAN and AOP respectively. Graphs have a logarithmic y-axis because, otherwise, with linear axis, the line of each case would not be well distinguished by the others, especially for those with higher accuracy.

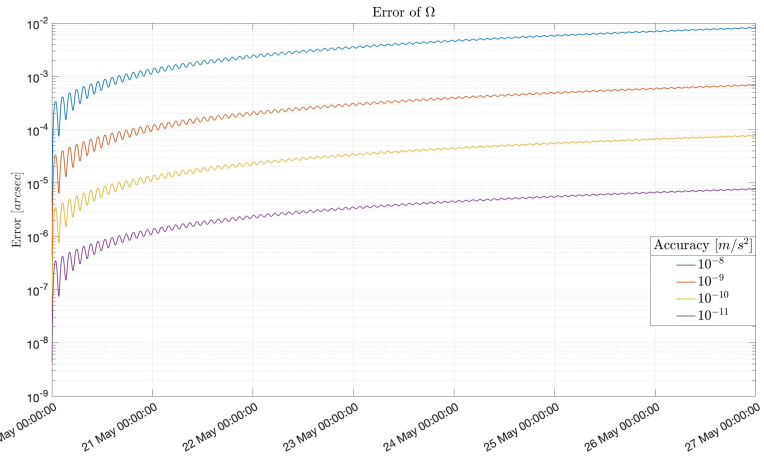

Figure 63: Absolute errors of RAAN expressed in arcsec

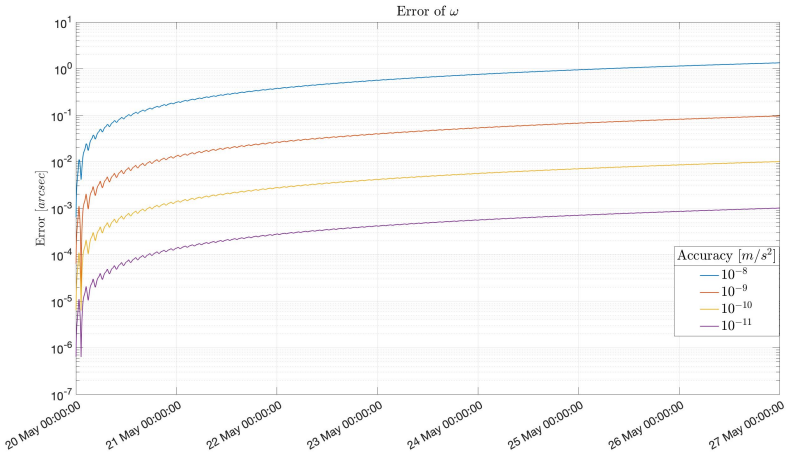

Figure 64: Absolute errors of AOP expressed in arcsec

It's possible to see that RAAN and AOP of each situation initially are quite coincident with the reference case (lines goes towards small values on the left), while the errors increase with time because of the continuous effects of drag and SRP. Moreover if the accelerometer is more accurate, the non measured contributions of non-gravitational forces are lower and the results of post-flight computation better approach those due to relativity (lower errors).
Through a linear fitting, with the least squares method, both Ω (RAAN) and ω (AOP) can be approximated by a straight line. The angular coefficients of these lines indicate the derivatives of the two parameters and so their variations in time. However the drifts are initially expressed as variations of angles per unit time, but, since POD makes metrical measurements, the drifts have to be converted in variation of length per unit time in order to understand what has to be expected when the tacking will be done.

Case	$\dot{\Omega}$	$\dot{\omega}$
1	15.078 $m/year$	-3.346 $°/day$
2	2.410 $m/year$	-227.163 $m/year$
3	0.877 $m/year$	29.812 $m/year$
4	0.752 $m/year$	47.704 $m/year$
5	0.737 $m/year$	49.584 $m/year$
6	0.736 $m/year$	49.793 $m/year$

Table 2: Drifts of the different cases.

As reported in Table 2, the first case presents a high value of drift of AOP but a small value of drift of RAAN. These results are coherent with the theory (see [8]),

because the nodal line of a polar orbit isn't influenced by even terms of gravity expansion, but it is influenced only by non-gravitational and relativistic effects, which are quite small. For what concerns the AOP, instead, it varies quickly especially due to the effect of J_2. Its results is not expressed as variation of length per unit time, because it's quite high.
For the other cases it's possible to see how the results are more and more closer to the case that considers only the spherical term of gravity and the relativistic effects (last line of the table), confirming what has been previously said about the increasing of accuracy. Moreover the drifts are of the order of some tens of $cm/year$ for RAAN and tens of $m/year$ for AOP, so they're measurable with POD (which has an accuracy of some centimeters).

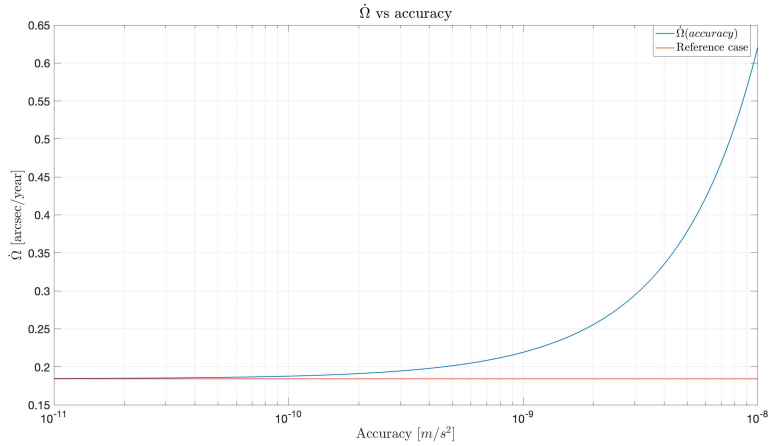

Figure 65: Drift of RAAN as function accuracy

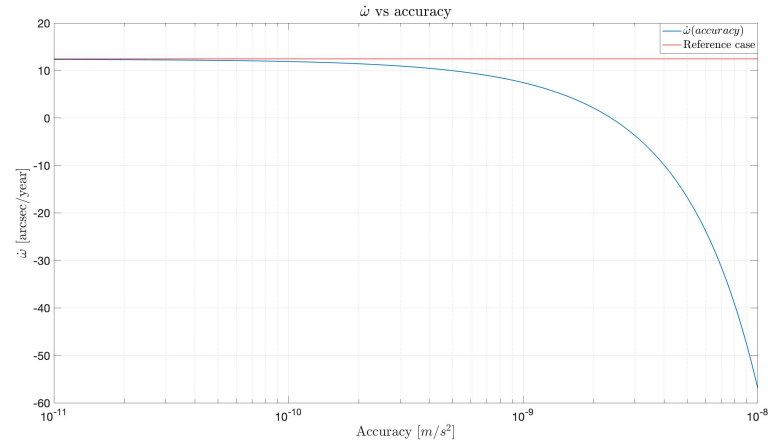

Figure 66: Drift of AOP as function accuracy

Figures 65 and 66 shows the behaviour of the drifts with respect to accuracy. Increasing the accuracy (moving to the left in the Figures) the blue line (the drift as

function of accuracy) gets always closer to an horizontal asymptote, in correspondence of the respective value of drift due to only relativistic effects.
It is also possible to compute the relative errors done on each drift as function of the accuracy with respect to the reference case (spherical gravity and relativity). The relative errors are expressed in percentage and are computed as:

$$\begin{aligned} e_{\dot{\Omega}_i} &= \frac{\dot{\Omega}_i - \dot{\Omega}_{ref}}{\dot{\Omega}_{ref}} \cdot 100 \\ e_{\dot{\omega}_i} &= \frac{\dot{\omega}_i - \dot{\omega}_{ref}}{\dot{\omega}_{ref}} \cdot 100 \end{aligned} \tag{27}$$

So after having computed the relative error for each case and making an interpolation of the obtained values, it's possible to represent how the relative error changes with respect to accuracy.
Figures 67 and 68 confirm that with higher accuracy the accelerations due to non-gravitational forces are better measured and then the relativistic effects can be estimate with more precision. Indeed the relative error tends to decrease towards smaller threshold values, i.e. towards higher accuracy, because the evaluated drifts converge to the drifts due to only relativity.

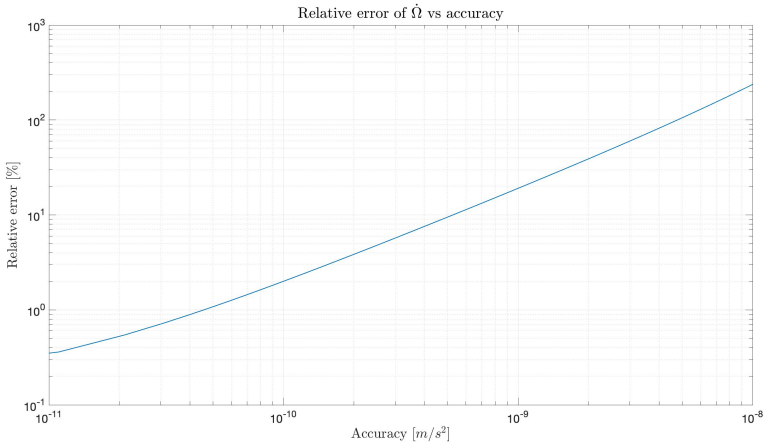

Figure 67: Relative error in drift of RAAN as function accuracy

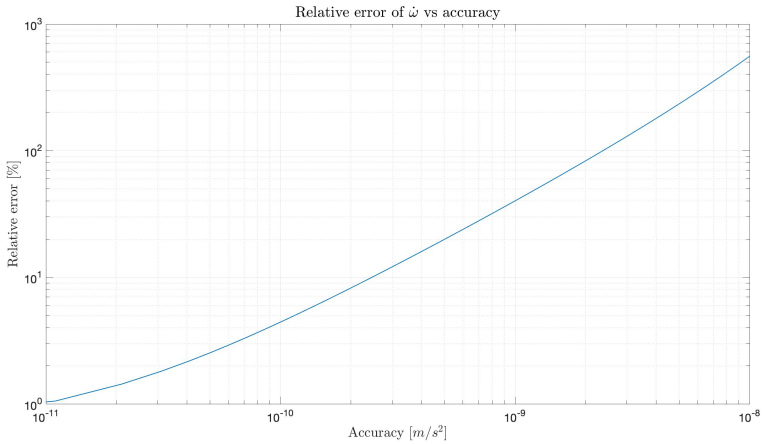

Figure 68: Relative error in drift of AOP as function accuracy

7 Accelerometer's characteristics

Considering all data collected both from dynamical simulations, spectral analysis and orbital analysis the required characteristics of the on-board accelerometer for the METRIC mission can be chosen: dynamic range (the interval of accelerations that the accelerometer can measure), bandwidth (the band of signal's frequencies in which the instrument collects data) and accuracy (how much the single measure differs from the "real" one).
Also accelerometers of previous missions have been considered to establish the feasibility of the instrument and its characteristics.
The following Table resumes the principal fetaures of the accelerometers of CHAMP, GRACE, GOCE and Bepi Colombo missions.

Mission	Dynamic range $[m/s^2]$	Bandwidth $[Hz]$	Accuracy $[m/s^2]$
CHAMP	$\pm 10^{-4}$	10^{-4} to 10^{-1}	$3 \cdot 10^{-9}$ for two axes $3 \cdot 10^{-8}$ less sensitive axis
GRACE	/	$2 \cdot 10^{-4}$ to 10^{-1}	$3 \cdot 10^{-10}$ for two axes $3 \cdot 10^{-9}$ less sensitive axis
GOCE	$\pm 3 \cdot 10^{-6}$	$5 \cdot 10^{-3}$ to 10^{-1}	10^{-12}
Bepi Colombo	$\pm 3 \cdot 10^{-6}$	$3 \cdot 10^{-5}$ to 10^{-1}	10^{-8}

Table 3: Dynamic characteristics of accelerometers of the past

As shown in the Table, CHAMP's accelerometer (STAR by ONERA) and also SuperSTAR, by ONERA again, of GRACE have good characteristics and also similar to each other, though dynamic range of SuperSTAR hasn't been found.
EGG accelerometer of GOCE is the most accurate between the accelerometers presented, but it has the narrower bandwidth.
The last is the Italian Spring Accelerometer (ISA) [2], illustrated in Figure 69, which is mounted on board of the satellite of Bepi Colombo mission [9]. ISA presents a large dynamic range for the non-gravitational accelerations, the wider bandwidth (with respect to the other accelerometers considered) and a good accuracy.

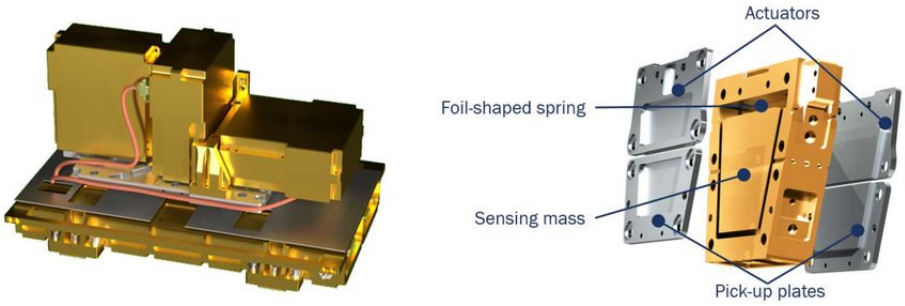

Figure 69: ISA accelerometer. Credit: Thales Alenia Space

From the measurements of non-gravitational accelerations acting on METRIC, the range of the accelerometer can be established, considering also the values in Table 3.

The proposed range is of $\pm 10^{-6}$ m/s^2 in order to have also a safety margin with respect to the highest simulated peaks of accelerations which are of about $2.4 \cdot 10^{-7}$ m/s^2. So, assuming a larger range, the accelerometer is able to measure all non-gravitational accelerations. Furthermore, the chosen range is smaller than those of Bepi Colombo and GOCE, so it's feasible.

For what concerns the bandwidth, observing the Figures of spectral analysis, it can be thought to have the lower extreme at 10^{-4} Hz, so that the contributions that are modulated with orbital frequency can be measured, and the higher extreme at 10^{-1} Hz as all others missions. Moreover, remember that accelerations that have a lower frequency than 10^{-4} Hz can be measured thanks to the spin of the satellite which allows to modulate those contributions with an higher frequency.

In the end the accuracy can be evaluated starting from the considerations relative to POD. Analyzing the Figures that represent drifts and their relative errors, the proposed accuracy is of 10^{-10} m/s^2, which is also feasible if compared with the values in Table 3. With this accuracy the drifts of RAAN and AOP due to only general relativity can be estimated with a good precision (relative errors respectively of $\sim 2\%$ and $\sim 4\%$), because the contributions of drag and SRP, that will be removed from tracking data, approximate very well their "real" values.

So, the proposed characteristics for the accelerometer are resumed in the Table below.

Dynamic range $[m/s^2]$	Bandwidth $[Hz]$	Accuracy $[m/s^2]$
$\pm 10^{-6}$	10^{-4} to 10^{-1}	10^{-10}

Table 4: Proposed characteristics for accelerometer of METRIC

As above stated, the accelerometer that will be mounted on-board of METRIC satellite will be a three axis accelerometer. So it will foresee three accelerometers mutually orthogonal one to the others, and each one must have the aforementioned features.

8 Conclusions

This thesis focuses on the study of the proposed METRIC mission, in particular on the payload of the satellite (the 3-axis accelerometer) and on the modelling of non-gravitational and relativistic effects. The accelerometer must be performant to allow reaching the mission's objectives; this instrument measures the non-gravitational accelerations acting on the spacecraft to improve the knowledge of atmospheric density, general relativity and geodesy. Because of these goals, it requires high accuracy, the necessary dynamic range and frequency bandwidth, features that must be evaluated as well as possible.

In order to evaluate how to reach these characteristics, METRIC mission's architecture has been studied (orbit, spacecraft's shape, etc), comparing it also with other missions flown around the Earth with similar goals or instruments on-board. In this way a full scenario of the current state of art has been achieved.

Accurate computations and simulations were needed and the publicly-available software (e.g. GMAT), proved not to be reliable to evaluate some of the very small effects at play and a new software had to be developed. After considering pros and cons, the choice of the software fell on Matlab©. In this programming environment, an orbital simulator was implemented. It is based on known dynamical models of gravity, drag, solar radiation pressure (SRP) and general relativity, that are the contributions that concern the objectives of the mission. Simulations have given as output both the accelerations that accelerometer will measure and the relativistic effects that are not measured by the accelerometer, in order to evaluate their relative weights on the perturbation of orbit.

The results have been then analyzed in terms of amplitude, evaluating their order of magnitude (showing that drag effects are the most important when the satellite passes near the perigee, but they're negligible near the apogee where SRP dominates), and also in term of frequency spectrum.

Since METRIC will be tracked with SLR from ground, the drifts of Right Ascension of Ascending Node (RAAN) and the Argument of Perigee (AOP) have been estimated through longer simulations, in order to understand if this technique may be useful in the reconstruction of relativistic effects. As a conclusion, a very good approximation is reachable if the accelerometer has the appropriate accuracy, so that it will measure non-gravitational accelerations precisely and their effects can be removed making it possible the evaluation of the relativistic contributions.

Finally the required characteristics of the three axis accelerometer were found, comparing them also with the respective features of other mission's accelerometers in

order to assess the feasibility of the instrument. The required accelerometer's characteristics were evaluated as follows:

- dynamic range: $\pm 10^{-6}\ m/s^2$;
- bandwidth: from $10^{-4}\ Hz$ to $10^{-1}\ Hz$;
- accuracy: $10^{-10}\ m/s^2$.

This work represents only a first iteration towards the final design of the accelerometer, though it's a good starting point for further analyses aimed at improving the results. First of all the simulator can be refined, in particular considering other numerical integrators with even higher accuracy and possibly speed of execution. Then also longer simulations can be considered (that last one year or more), so that the effects that vary in long periods, like SRP, can be better evaluated.

9 Acknowledgement

Foremost I would like to thank my supervisor Professor Enrico Lorenzini for the support he has given me step by step since the first day I started this thesis. He was always available and patient with me when I needed his help. I really express my gratitude for his enthusiasm and also for the confidence in me, because he allowed me to work on this special mission knowing also other important people.
The assistance provided by Professor Andrea Valmorbida was greatly appreciated too. He gave me some important advice not only for this thesis but also for my career and I won't forget them.
I wish to acknowledge all my mates, especially Lorenzo, who passed with me five unforgettable years between projects, laughs, hours passed in study rooms, lunches together and so on.
My sincere appreciation goes also to my friends and football teammates, because they were able to help me in having fun and make the study less heavy.
I'm really grateful to Giorgia, because, in spite of everything, she was always with me, also in my worst moments. She always gave me the better advice and if I reach this goal, it's also thank to her support.
I would like to acknowledge my family for the assistance in every situation of all my daily life. My grandmother, my uncles, my cousin Francesco were always ready to help and encourage me to do my best.
Last but not least, I'm mostly thankful to my parents. They made me who I am, giving me the best part of them. I'm proud because they were, they are and they will be the reason of my successes. Without them I wouldn't have been able to reach my target.

10 Bibliography

Papers/Articles/Report

[1] Enrico Lorenzini, Roberto Peron. "METRIC: a dedicated Earth-orbiting spacecraft for fundamental physics and geophysics". In: *IEEE Xplore* (2018). DOI: 10.1109/MetroAeroSpace.2018.8453539.

[2] Francesco Santoli, Emiliano Fiorenza, Carlo Lefreve, David Massimo Lucchesi, Marco Lucente, Carmelo Magnafico, Alfredo Morbidini, Roberto Peron, Valerio Iafolla. "ISA, a High Sensitivity Accelerometer in the Interplanetary Space". In: *Space Science Reviews* (2020). DOI: https://doi.org/10.1007/s11214-020-00768-6.

[3] NASA. "General Mission Analysis Tool (GMAT) User Guide". In: (2020). URL: https://gmat.sourceforge.net/docs/R2020a/help-a4.pdf.

[4] NASA. "Satellite Laser Ranging and Earth Science". In: (). URL: https://ilrs.gsfc.nasa.gov/docs/slrover.pdf.

[5] Oliver Montenbruck, Remco Kroes. "In-flight performance analysis of the CHAMP BlackJack GPS Receiver". In: *GPS Solutions* 7.2 (2003). DOI: 10.1007/s10291-003-0055-5.

[6] Roberto Peron, Enrico Lorenzini. "METRIC: A Dedicated Earth-Orbiting Spacecraft for Investigating Gravitational Physics and the Space Environment". In: *Aerospace* (2017). DOI: https://doi.org/10.3390/aerospace4030038.

Books

[7] David A. Vallado. *Fundamentals of Astrodynamics and Application*. Space Technology Library. Microcosm Press, 2013. ISBN: 9781881883180.

[8] Howard D. Curtis. *Orbital Mechanics for Engineering Students*. Elvesier Aerospace Engineering Series. 2009. ISBN: 9780080887845.

Website

[9] ESA. *bepicolombo*. URL: https://www.esa.int/Science_Exploration/Space_Science/BepiColombo. (last view: 19.11.2022).

[10] ESA. *CHAMP*. URL: https://www.eoportal.org/satellite-missions/champ#star-space-three-axis-accelerometer-for-research-mission. (last view: 07.10.2022).

[11] ESA. *GOCE*. URL: https://www.eoportal.org/satellite-missions/goce#eop-quick-facts-section. (last view: 10.10.2022).

[12] ESA. *GRACE*. URL: https://earth.esa.int/eogateway/missions/grace. (last view: 05.10.2022).

[13] ESA. *GRACE*. URL: https://www.eoportal.org/satellite-missions/grace#grace-gravity-recovery-and-climate-experiment. (last view: 07.10.2022).

[14] JPL. *LAGEOS 1,2*. URL: https://web.archive.org/web/20110721062751/http://space.jpl.nasa.gov/msl/QuickLooks/lageosQL.html. (last view: 03.10.2022).

[15] LARES. *LARES Mission*. URL: https://www.lares-mission.com/LARES.asp. (last view: 10.10.2022).

[16] NASA. *CHAMP*. URL: https://nssdc.gsfc.nasa.gov/nmc/spacecraft/display.action?id=2000-039B. (last view: 03.10.2022).

[17] NASA. *LAGEOS: LASser GEOdynamic Satellite*. URL: https://lageos.gsfc.nasa.gov. (last view: 07.10.2022).